Climate Dynamics (2024) 62:10599–10620
https://doi.org/10.1007/s00382-024-07465-y

ORIGINAL ARTICLE

Arctic climate feedback response to local sea-ice concentration and remote sea surface temperature changes in PAMIP simulations

Matthew T. Jenkins[1] · **Aiguo Dai**[1] · **Clara Deser**[2]

Received: 23 December 2023 / Accepted: 1 October 2024 / Published online: 30 October 2024

Keywords Arctic amplification · Sea-ice loss · Climate feedback · Global warming · Arctic warming · Ocean heat release · Atmospheric energy transport

1 Introduction

The Arctic region warms faster than the rest of the world in response to increased greenhouse gas (GHG) concentrations – a phenomenon known as Arctic amplification (AA) (Serreze and Barry 2011; Walsh 2014; England et al. 2021; Taylor et al. 2022). Many mechanisms have been proposed to explain AA such as surface albedo feedback (Hall 2004; Winton 2006), increased surface downwelling longwave (LW) radiation from enhanced poleward energy transport (Cai 2005; Henry et al. 2021), increased water vapor, clouds (Barton and Veron 2012; Ghatak and Miller 2013; Burt et al. 2016; Gong et al. 2017; Monroe et al. 2021), and the positive lapse rate feedback (Pithan and Mauritsen 2014; Goosse et al. 2018), and increased upward oceanic energy fluxes due to sea-ice loss (Deser et al. 2010; Kumar et al. 2010; Screen and Simmonds 2010a, b; Boeke and Taylor 2018; Dai et al. 2019; Sejas and Taylor 2023). The local and remote mechanisms suggested to contribute to AA are tightly coupled (Feldl et al. 2017b; Henry et al. 2021; Dai and Jenkins 2023), making the exact causes of AA unclear in a fully coupled system. For instance, sea-ice loss largely shapes the spatial patterns of Arctic surface warming and positive lapse rate feedback (Feldl et al. 2020; Boeke et al 2021) by increasing upward surface energy fluxes in autumn and winter that in turn influences Arctic atmospheric energy convergence and LW cloud feedbacks in non-summer months (Jenkins and Dai 2021). Further, warming in low-mid latitude regions influences Arctic mid-upper tropospheric warming through changes in atmospheric energy convergence into the Arctic, affecting the structure of Arctic warming profiles and lapse rate feedback (Perlwitz et al. 2015; Feldl et al. 2020; Hay et al. 2022). Additionally, Liang et al. (2022) showed that AA weakens in the future for greater CO_2 concentrations due to weaker Arctic and global warming differences. Thus, more work is needed to understand how local and remote processes influence Arctic warming and AA.

Arctic sea-ice loss plays an essential role in local Arctic warming (Dai et al. 2019; Linke et al. 2023b) and may contribute to warmer winters in northern hemisphere mid-latitude areas (Sun et al. 2016). As sea-ice retreats, increased energy transfer from warm, open water surfaces to the frigid overlying atmosphere during polar night contributes to large AA (Kumar et al. 2010; Deser et al. 2010; Screen and Simmonds 2010a, b; Boeke and Taylor 2018; Taylor et al. 2018; Dai et al. 2019; Dai and Jenkins 2023). Exclusion of sea-ice loss effects from models greatly weakens AA. Specifically, Dai et al. (2019) showed that AA weakens in model experiments with 1%/year CO_2 increases and fixed SIC for surface flux calculations, and that negligible additional AA will occur after sea-ice completely melts away. Davy and Griewank (2023) confirmed this finding by showing that as the rate of sea-ice loss decreases in the future, concurrent AA weakens. Lastly, previous studies suggest that increased surface heat capacity associated with sea-ice loss affects AA seasonality because more energy input (release) is required to raise (cool) the temperature of open water than sea ice (Dwyer et al. 2012; Hahn et al. 2022; Hu et al. 2022; Sejas and Taylor 2023). Thus, the reduced ice-insulation effect associated with sea-ice loss (Deser et al. 2010; Dai et al. 2019; Dai and Jenkins 2023) and changes in the effective oceanic heat capacity (Hahn et al. 2022; Sejas and Taylor 2023) establish the seasonality of AA.

✉ Matthew T. Jenkins
mtjenkins@albany.edu

[1] University at Albany, State University of New York, Albany, NY, USA

[2] National Center for Atmospheric Research, Boulder, CO, USA

Another process underlying AA is the lapse rate feedback that depends on local vertical warming structures (Pithan and Mauritsen 2014; Linke et al. 2023a; Janoski et al. 2023; Zhou et al. 2023). Under a bottom-heavy warming profile, outgoing LW radiation at the top of the atmosphere (TOA) is reduced relative to vertically uniform warming, thereby enhancing surface warming (Boeke et al. 2021; Dai and Jenkins 2023). In contrast, a top-heavy warming profile, as seen in the tropics, suppresses surface warming by increasing outgoing LW radiation (Colman and Soden 2021). The lapse rate feedback has been considered as a major contributor to AA due to its large Arctic versus tropical warming effect (Pithan and Mauritsen 2014; Goosse et al. 2018; Hahn et al. 2021). Previous studies have attributed Arctic bottom-heavy warming and the resultant positive lapse rate feedback to high lower-tropospheric stability, which effectively traps warming at the surface (Bintanja et al. 2011; Pithan and Mauritsen 2014). However, recent studies suggest that Arctic lapse rate feedback is strongly correlated with surface warming patterns and sea-ice loss (Feldl et al. 2020; Boeke et al. 2021; Jenkins and Dai 2021) rather than stability strength (Jenkins and Dai 2022; Dai and Jenkins 2023). Remote processes, such as enhanced moist static energy convergence into the Arctic, may also influence Arctic lapse rate feedback by favoring warming in the mid-upper troposphere (Feldl et al. 2020), leading to negative lapse rate feedback.

During summer, surface albedo and water vapor feedbacks activate in the Arctic in response to greenhouse gas (GHG) forcing. The surface albedo feedback makes a large positive contribution to Arctic energy imbalance in summer (Hall 2004; Winton 2006; Pithan and Mauritsen 2014; Goosse et al. 2018; Hahn et al. 2021); however, most of the enhanced shortwave (SW) absorption preferably warms the ocean mixed layer rather than near-surface air (Dai 2021; Dai and Jenkins 2023). Additionally, water vapor feedback has been suggested to contribute to Arctic *warming* (Ghatak and Miller 2013; Gong et al. 2017) but oppose Arctic *amplification* due to larger moistening in tropical regions than polar areas under increased GHGs (Pithan and Mauritsen 2014; Hahn et al. 2021). Jenkins and Dai (2022) showed that water vapor feedback and sea-ice loss spatial patterns are weakly correlated in ERA5 reanalysis data, but they did not quantify the underlying local and remote drivers of Arctic water vapor feedback. An improved understanding of Arctic water vapor feedback is needed as it enhances Arctic surface warming and melts sea ice, indirectly contributing to AA through the sea-ice feedback (Dai et al. 2019; Dai and Jenkins 2023). Moreover, water vapor feedback may interact with other processes by changing patterns of atmospheric latent energy transport (Chung and Feldl 2023) or amplifying other climate feedbacks (Beer and Eisenman 2022).

Cloud feedback impacts TOA and surface energy fluxes (Wetherald and Manabe 1988), but their response to local and remote processes is not fully understood. Previous studies have found an increase in local Arctic low cloud amounts and cloud water content in response to local sea-ice loss due to strong cold season ocean–atmosphere coupling (Schweiger et al. 2008; Kay and Gettelman 2009; Eastman and Warren 2010; Palm et al. 2010; Liu et al. 2012; Taylor et al. 2015; Kay et al. 2016; Morrison et al. 2018, 2019; Jenkins and Dai 2022; Jenkins et al. 2023; Taylor and Monroe 2023). Increased surface downwelling LW radiation from local Arctic cloud increases slows sea ice growth during Arctic autumn and winter, lengthening exposure of open water surfaces to heat the overlying air during the cold season (Monroe et al. 2021). Nonlocal cloud feedbacks may also contribute to Arctic warming and AA by affecting remote surface warming patterns and thus atmospheric energy transport into the Arctic (Vavrus et al. 2004; Middlemas et al. 2020).

Increased energy transport from midlatitudes into the Arctic has been suggested to influence AA (Cai 2005; Roe et al. 2015; Feldl et al. 2017b; Soldatenko 2021). Without sea-ice loss and associated surface heating, enhanced poleward atmospheric energy transport produces only weak AA in model simulations (Alexeev et al. 2005; Merlis and Henry 2018; Henry et al. 2021). On the other hand, inclusion of sea-ice loss effects in model simulations reduces atmospheric energy transport into the Arctic due to decreased temperature gradients between middle and high latitudes (Hwang et al. 2011; Jenkins and Dai 2021; Audette et al. 2021; Hahn et al. 2023). However, Cardinale and Rose (2023) showed that an increase in the fraction of the Arctic energy convergence used to heat the surface may overcome the total decrease in Arctic energy convergence, contributing to winter Arctic warming. Inhomogeneous spatial patterns of radiative forcing also influence atmospheric poleward energy transport (Stuecker et al. 2018; Virgin and Smith 2019). When radiative forcing is negative in the Arctic, atmospheric poleward energy transport increases to offset the energy imbalance, inducing small AA (Virgin and Smith 2019). Additionally, Stuecker et al. (2018) found that atmospheric energy transport became an important contributor to AA in response to radiative forcing applied only in midlatitudes in fully coupled simulations, but they did not examine the effects of sea-ice loss in shaping the Arctic warming in response to such forcing.

The relative importance of sea-ice loss, positive climate feedbacks, and atmospheric energy transport in shaping AA is still debated and merits further investigation. Arctic climate feedbacks have been estimated in coupled model simulations (Pithan and Mauritsen 2014; Sejas et al. 2014; Goosse et al. 2018; Stuecker et al. 2018; Previdi et al. 2020; Hahn et al. 2021); however, the influence of local sea-ice loss or remote SST warming on climate feedbacks cannot be explicitly quantified in a fully coupled system. To

address these points, we use atmosphere-only simulations from the Polar Amplification Model Intercomparison Project (PAMIP; Smith et al. 2019) to answer the following questions:

1. What are the impacts of local Arctic SIC changes through enhanced oceanic heating of the atmosphere versus impacts of global SST changes and background warming in atmosphere-only model simulations on Arctic surface warming, AA, radiative climate feedbacks, and atmospheric energy transport?
2. Do the individual responses to SST warming or Arctic SIC loss sum to the total response to the combined influences of SST warming and Arctic SIC loss occurring simultaneously?

The PAMIP experiments allow us to separate the climate response to perturbations in local sea ice or remote SST changes in model simulations under fixed GHG concentrations. The SST perturbation runs represent the climatic effects of background global warming without large AA, while the Arctic SIC change simulations show the impact from Arctic sea-ice loss without background global warming.

2 Methods

2.1 PAMIP experiments

We investigate how changes in global SST and/or local SIC impact Arctic surface warming, AA, climate feedbacks, and atmospheric energy transport using PAMIP atmosphere-only time slice experiments (Table 1; Smith et al. 2019). PAMIP experiment 1.1 (pdSST-pdSIC) serves as the control run where global SST and polar (i.e., Arctic and Antarctic) SIC fields are fixed at their present-day (pd) (i.e., year 2000) values. To isolate the response to global SST changes, we compare the pdSST-pdSIC run to PAMIP experiments 1.3 (piSST-pdSIC) and 1.4 (futSST-pdSIC) where polar (i.e., Arctic and Antarctic) SIC remains fixed at present-day conditions and SSTs over open water surfaces are set to preindustrial (pi) and future (fut) states (defined below), respectively. Likewise, we difference the pdSST-pdSIC run with PAMIP experiments 1.5 (pdSST-piArcSIC) and 1.6 (pdSST-futArcSIC) where SSTs outside the Arctic region are fixed at their present-day values and Arctic SIC is changed to preindustrial and future states to separate the impacts of sea-ice loss from other forcings. For the pdSST-piArcSIC and pdSST-futArcSIC simulations, SSTs are specified at their preindustrial or future values in regions where preindustrial or future SIC deviates by more than 10% of the present-day state, respectively (Smith et al. 2019).

Figure 1 shows the maps of prescribed SST and SIC changes for the preindustrial (Fig. 1a, b) or future (Fig. 1c, d) cases. To facilitate comparison with the future changes, which are relative to present-day, the historical changes are computed as present-day minus preindustrial in Fig. 1 and all other figures. We also compute the difference between pdSST-pdSIC and experiment 1.2 (piSST-piSIC; referred to as TOTAL) where global SSTs and polar SIC are changed simultaneously to their preindustrial states. We compare the results from TOTAL to the difference between pdSST-pdSIC and the sum of piSST-pdSIC, pdSST-piArcSIC and pdSST-piAntSIC (referred to as SUM) to assess the linearity of the total climate response to both polar SIC and global SST changes. The preindustrial, present-day, and future time periods correspond to estimated Arctic SIC and/or global SST conditions under global-mean surface temperatures of 13.67 °C, 14.24 °C, and 15.67 °C, respectively (Smith et al. 2019), which correspond to a historical warming of 0.57 °C and a future warming of 1.43 °C relative to present-day. Their corresponding SIC changes are also much larger for the future case than the historical case (Fig. 1). Present-day SST and SIC fields are based on the 1979–2008 climatology from the Hadley Center Sea Ice and Sea Surface Temperature dataset (HadISST; Rayner et al. 2003). Preindustrial and future SST and SIC fields are derived from the CMIP5 historical and RCP8.5 experiments for 31 models, respectively (Smith et al. 2019). See Appendix A of Smith et al. (2019) for more details.

We use monthly-mean output from five models (i.e., AWI-CM1-1-MR, CESM2, CNRM-CM6-1, CanESM5, IPSL-CM6A-LR) that provided the necessary fields for our analysis. AWI-CM1-1-MR and CNRM-CM6-1 did not output the necessary variables for some calculations in piSST-piSIC (i.e., TOTAL) and is excluded in our comparison of piSST-piSIC to the sum of piSST-pdSIC, pdSST-piArcSIC, and pdSST-piAntSIC (i.e., SUM). Each model and experiment are initialized on 1 April 2000 and are run for 14-months, discarding the first two months as spin-up (Smith et al. 2019). To improve robustness of the results, we analyze the ensemble mean of the 100 ensemble runs with varied initial conditions for each model and experiment as atmospheric internal variability can mask the climatic response to SIC or SST changes (Screen et al. 2014). We define the Arctic region as the area poleward of 67° N following previous work (e.g., Dai et al. 2019; Jenkins and Dai 2022) because most Arctic sea-ice exists poleward of this latitude and the Arctic is mostly ocean surface in this region. We exclude land surfaces in our Arctic regional averages because surface warming is strongest over oceanic areas (Boeke and Taylor 2018; Dai et al. 2019) but inclusion of land areas does not qualitatively affect our results. Globally averaged fields include both land and ocean surfaces. For this study, we calculate AA as the difference between Arctic (excluding land) and global surface air temperature (ΔT_{as}) changes ($AA = \Delta T_{as,ARCTIC} - \Delta T_{as,GLOBAL}$) rather than as the

Table 1 Summary of PAMIP experiments used in the analysis (from Smith et al. 2019)

Model Simulation	Full Name	Description
1.1 pdSST-pdSIC	Present day sea surface temperature Present-day sea-ice concentration	Year 2000 global SST and polar SIC; control run
1.2 piSST-piSIC	Preindustrial sea surface temperature Preindustrial sea-ice concentration	Historical global SST and polar SIC; assesses total climate response to SST and SIC changes
1.3 piSST-pdSIC	Preindustrial sea surface temperature Present-day sea-ice concentration	Historical (1.3) and future (1.4) global SST with polar SIC fixed at year 2000 conditions; assesses role of background warming without sea-ice feedback
1.4 futSST-pdSIC	Future sea surface temperature Present-day sea-ice concentration	
1.5 pdSST-piArcSIC	Present-day sea surface temperature Preindustrial sea-ice concentration	Historical (1.5) and future (1.6) Arctic SIC with global SST fixed at year 2000 conditions; assesses role of Arctic sea-ice feedback without background warming
1.6 pdSST-futArcSIC	Present-day sea surface temperature Future sea ice concentration	
1.7 pdSST-piAntSIC	Present-day SST Preindustrial Antarctic SIC	Historical Antarctic SIC with global SST fixed at year 2000 conditions; assesses role of Antarctic sea-ice feedback without background warming

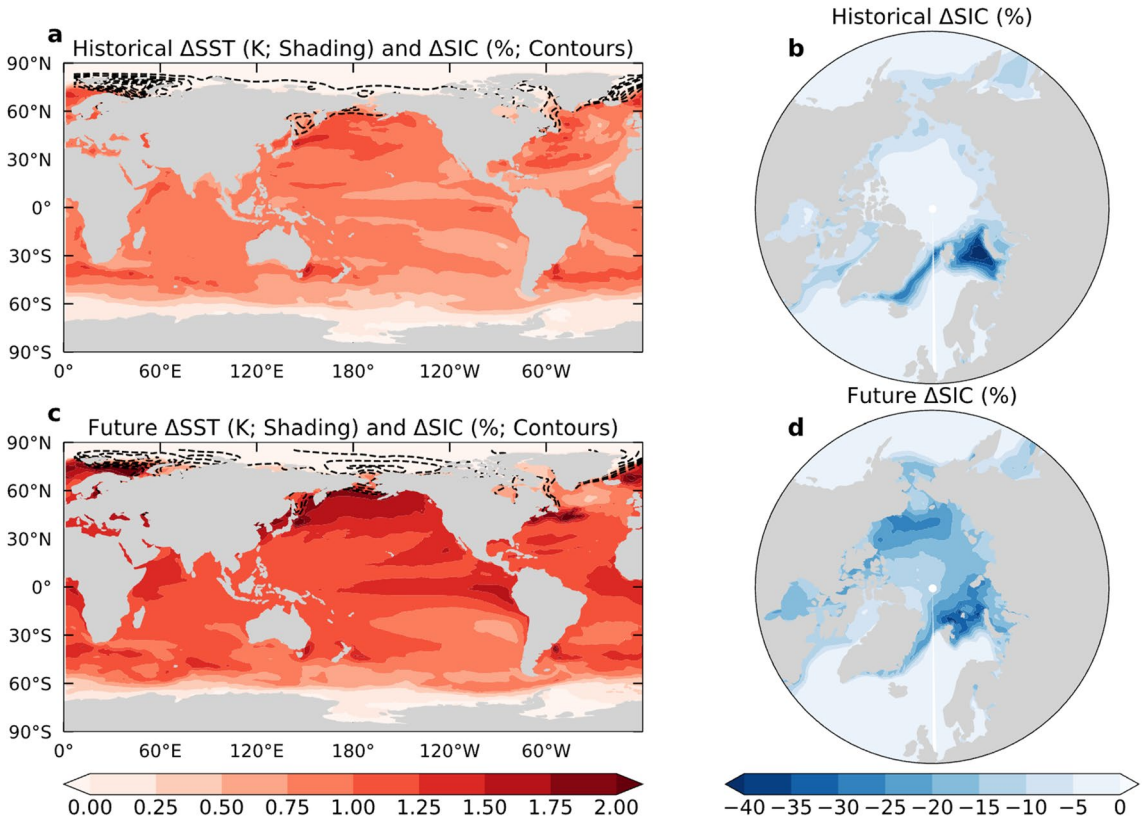

Fig. 1 **a**, **c** Annual mean changes in SST (K; shading) and Arctic SIC (%; contours; interval 5%) for the **a** historical (present-day minus preindustrial) and **c** future warming (future minus present-day) cases. Changes in SIC for the **b** historical and **d** future cases are shown as shading in **b**, **d** for clarity

ratio of Arctic to global warming to avoid dividing by near-zero values for global-mean surface air temperature changes.

2.2 Energy budgets

The vertically integrated energy budget equation (Eq. 1) for an atmospheric column accounts for the net TOA radiative flux

($R^{\downarrow}_{TOA}$; positive downward), net surface energy flux ($R^{\downarrow}_{SFC}$; positive downward), change in local energy storage in the atmospheric column ($\frac{\partial E}{\partial t}$), and horizontal convergence of energy ($-\nabla \bullet \boldsymbol{F}_A$) (Trenberth 1997; Fasullo and Trenberth 2008):

$$\frac{\partial E}{\partial t} = R^{\downarrow}_{TOA} - R^{\downarrow}_{SFC} - \nabla \cdot \boldsymbol{F}_A, \tag{1}$$

where

$$E = \frac{1}{g}\int_{p_{TOA}}^{p_s} \left(c_p T + Lq + gz\right) dp. \tag{2}$$

In Eq. (2), E is the vertically integrated moist static energy, where c_pT, Lq, and gz denote atmospheric internal energy, latent energy, and potential energy, respectively. Atmospheric kinetic energy storage is small and is not included in Eq. (2), following previous studies (Oort and Vonder Haar 1976; Trenberth and Solomon 1994). For the flux terms, we calculate $R^{\downarrow}_{TOA}$ and $R^{\downarrow}_{SFC}$ as:

$$R^{\downarrow}_{TOA} = ASR^{\downarrow} - OLR^{\uparrow} \tag{3}$$

$$R^{\downarrow}_{SFC} = SW^{\downarrow}_{NET,SFC} - LW^{\uparrow}_{NET,SFC} - SH^{\uparrow} - LH^{\uparrow} \tag{4}$$

where $ASR^{\downarrow}$, $OLR^{\uparrow}$, $SW^{\downarrow}_{NET,SFC}$, $LW^{\uparrow}_{NET,SFC}$, $SH^{\uparrow}$, and $LH^{\uparrow}$ are the TOA absorbed SW radiation (positive downward), TOA outgoing LW radiation (positive upward), net surface SW radiation (positive downward), net surface LW radiation (positive upward), surface sensible and latent heat flux (positive upward), respectively. Note that the latent heat term does not account for the latent heat consumed in snow melt in Eq. (4). To estimate oceanic heat uptake (OHU), we calculate the net surface energy flux (Eq. 4) over ocean surfaces only. In regions where SSTs are specified in both sets of simulations, changes in OHU implicitly include changes in oceanic energy convergence in addition to oceanic heat storage changes as historical and future SST values are obtained using a coupled atmosphere–ocean. However, the OHU term in the simulations with perturbed Arctic SIC and fixed global SST is dominated by seasonal oceanic heat storage changes (Dai 2021; Hu et al. 2022). We also note that the OHU term in the future Arctic SIC simulations implicitly includes effects from reduced ice heat transport as sea ice melting weakens sea ice export in fully-coupled climate runs (Kay et al. 2012).

We compute the horizontal atmospheric energy convergence ($-\nabla \bullet \boldsymbol{F}_A$) by rearranging the terms in Eq. (1) to obtain:

$$-\nabla \cdot \boldsymbol{F}_A = R^{\downarrow}_{SFC} - R^{\downarrow}_{TOA} + \frac{\partial E}{\partial t}. \tag{5}$$

Equation (5) shows that the net convergence of the horizontal energy flux (in W m^{-2}) into an atmospheric column is linked to the difference between the energy absorbed at the surface and net TOA radiation, and changes in local energy storage. Note that the local energy storage term is calculated using a month-to-month time derivative of Eq. (2) and is necessary for calculating monthly energy convergence but sums to zero in the annual mean. We also calculate the atmospheric energy transport (AET; in PW) into the region north of a given latitude (ϕ) by taking the area integral of the net energy convergence over the region following previous studies (Hwang and Frierson 2010; Feldl et al. 2017a):

$$AET(\phi) = \int_{\phi}^{\pi/2}\int_{0}^{2\pi} \left(R^{\downarrow}_{SFC} - R^{\downarrow}_{TOA} + \frac{\partial E}{\partial t}\right) a^2 cos\phi d\gamma d\phi. \tag{6}$$

In Eq. (6), a is the radius of Earth (~6.371×10^6 m), γ is the longitude, and ϕ is the latitude. $AET(\phi)$ represents the total energy crosses the latitude circle at ϕ (positive northward). For our Arctic region, ϕ = 67°N.

2.3 Climate feedback calculations

The response of the atmospheric energy budget to a climate perturbation, assuming negligible changes in atmospheric energy storage, is:

$$\Delta R^{\downarrow}_{TOA} - \Delta R^{\downarrow}_{SFC} - \Delta\left(\nabla \cdot \boldsymbol{F_A}\right) = 0 \tag{7}$$

where $\Delta R^{\downarrow}_{TOA}$, $\Delta R^{\downarrow}_{SFC}$, and $\Delta\left(\nabla \bullet \boldsymbol{F_A}\right)$ are changes in the net TOA radiative flux, net surface energy flux, and atmospheric horizontal energy convergence at each grid point, respectively (Stuecker et al. 2018; Hahn et al. 2021; Zhou et al. 2023). We use the Pendergrass et al. (2018) CESM1-CAM5 radiative kernels to decompose changes in the TOA net radiative flux into individual contributions from changes in surface albedo (ΔR_α), water vapor (ΔR_q), air temperature (ΔR_T), and clouds (ΔR_C):

$$\Delta R^{\downarrow}_{TOA} = \Delta R^{\downarrow}_{\alpha} + \Delta R^{\downarrow}_{q} + \Delta R^{\downarrow}_{T} + \Delta R^{\downarrow}_{C}. \tag{8}$$

GHG concentrations remain fixed at year 2000 levels in the PAMIP simulations, so we exclude an effective radiative forcing term from our TOA flux change decomposition. The annual-mean residual TOA radiative flux changes (i.e., the difference between the actual TOA radiation change and sum of radiative feedback contributions in Eq. (8)) averaged over the Arctic are 0.29 W m^{-2} and 0.27 W m^{-2} for historical and future global SST changes with fixed SIC, and 1.15 W m^{-2} and 1.79 W m^{-2} for historical and future Arctic SIC with fixed global SST. The residual values mentioned above represent nonlinearities in climate feedback processes that are not captured by the kernel method and are relatively small compared to the individual feedback terms reported below. This suggests that the kernel method captures the change in

TOA radiation well for both experiments. We also normalize the TOA flux changes in Eq. (8) by the annual-mean *local* surface air temperature change (ΔT_{as}) to calculate the climate feedback parameter (λ_i) for each variable using:

$$\sum_i \lambda_i = \lambda_\alpha + \lambda_q + \lambda_T + \lambda_C = \frac{\Delta R_\alpha^{\downarrow} + \Delta R_q^{\downarrow} + \Delta R_T^{\downarrow} + \Delta R_C^{\downarrow}}{\Delta T_{as}} \tag{9}$$

For clarity, we use the term *feedback* to refer to the unnormalized TOA radiative flux changes (units: W m^{-2}) in Eq. (8) and *feedback parameter* to refer to the normalized TOA radiative fluxes (units: W m^{-2} K^{-1}) in Eq. (9).

Radiative kernels are computed by perturbing one climate variable in a radiative transfer model and keeping all other variables fixed to produce a TOA radiative flux response, which is divided by the amount of the perturbed variable change to derive the TOA flux change per unit variable change (Soden et al. 2008). To calculate the surface albedo feedback, we compute the product of the surface albedo kernel (K_α) and changes in surface albedo ($\Delta\alpha$): $\Delta R_\alpha = K_\alpha * \Delta\alpha$. For water vapor (Eq. 10) and temperature (Eq. 11) feedbacks, we vertically integrate the product of the kernel and change in each respective variable from the surface (p_s) to the tropopause (p_{TOA}):

$$\Delta R_q = \int_{p_{TOA}}^{p_s} K_q * \Delta \ln(q) dp \tag{10}$$

$$\Delta R_T = K_{Ts} * \Delta T_{as} + \int_{p_{TOA}}^{p_s} K_{T_a} * \Delta T_a dp \tag{11}$$

where q and T_a represent specific humidity and air temperature, respectively. Radiative emissions from water vapor scale with the natural logarithm of specific humidity, so we use $\Delta\ln(q)$ in Eq. (10) as done previously (Shell et al. 2008). Also, note that the temperature feedback accounts for changes in surface temperature, which is computed by taking the product of the surface temperature kernel (K_{Ts}) and change in surface air temperature (ΔT_{as}) (Block and Mauritsen 2013; Jenkins and Dai 2021). Further, we assume that the tropopause pressure increases with latitude from 100 hPa at the equator to 300 hPa at the poles following Pithan and Mauritsen (2014) to mask out the stratosphere. To calculate Planck and lapse rate feedbacks, we separate the temperature feedback (ΔR_T) into a component associated with vertically uniform warming equal to that of the surface (Planck feedback; ΔR_{PL}) and deviations from the vertically uniform warming profile (lapse rate feedback; ΔR_{LR}):

$$\Delta R_T = \Delta R_{PL} + \Delta R_{LR}$$

$$= K_{Ts} * \Delta T_{as} + \int_{p_{TOA}}^{p_s} K_{T_a} * \Delta T_{as} dp + \int_{p_{TOA}}^{p_s} K_{T_a} * (\Delta T_a - \Delta T_{as}) dp \tag{12}$$

More details on Planck and lapse rate feedback calculations are provided in Jenkins and Dai (2021) and Dai and Jenkins (2023).

The change in cloud radiative forcing (ΔCRF)—the difference between all-sky and clear-sky radiative fluxes—provides a simple estimate of the energetic effects of clouds but does not represent cloud feedback as other processes also affect this difference (Soden et al. 2008; Block and Mauritsen 2013). To compute cloud feedback (ΔR_C), we subtract a cloud masking (CM) term from the ΔCRF to account for the effects of changes in surface albedo, temperature, and water vapor on ΔCRF (Soden et al. 2008):

$$\Delta R_C = \Delta CRF - CM \tag{13}$$

where

$$M = \left(K_\alpha - K_\alpha^C\right) * \Delta\alpha + \int_{p_{TOA}}^{p_s} \left(K_{T_a} - K_{T_a}^C\right) * \Delta T_a dp + \int_{p_{TOA}}^{p_s} \left(K_q - K_q^C\right) * \Delta ln(q) dp. \tag{14}$$

In Eq. (14) K_i and K_i^C are the all-sky and clear-sky kernels for surface albedo (α), air temperature (T_a), and water vapor (q). GHG concentrations are fixed in the PAMIP runs so we exclude a GHG masking term in Eq. (14).

2.4 Potential warming contribution estimates

To facilitate comparison, we quantify climate feedbacks, oceanic heat uptake, and horizontal atmospheric energy convergence in terms of their *potential* warming contributions following previous studies (e.g., Pithan and Mauritsen 2014; Goosse et al. 2021; Stuecker et al. 2018; Hahn et al. 2021). The potential warming contribution from the *i*th climate feedback ($\Delta T_i = \Delta R_i / \overline{\lambda}_{PL}$, in K) represents a hypothetic warming amount needed to rebalance the TOA energy flux change ($\Delta R_i = \lambda_i \Delta T_{as}$) through the negative Planck feedback at a new *equilibrium* state. Similarly, we can scale the other flux changes to estimate their potential warming contributions, and the total potential warming amount (ΔT) is estimated as (Goosse et al. 2018; Hahn et al. 2021):

$$\Delta T = -\frac{\sum_i \lambda_i \Delta T_{as}}{\overline{\lambda}_{PL}} - \frac{\lambda_{PL}' \Delta T_{as}}{\overline{\lambda}_{PL}} - \frac{\Delta(-\nabla \bullet \boldsymbol{F_A})}{\overline{\lambda}_{PL}} - \frac{\Delta OHU}{\overline{\lambda}_{PL}} \tag{15}$$

where $\overline{\lambda}_{PL}$ (in W m^{-2} K^{-1}) is the global-mean Planck feedback parameter and λ_{PL}' is the deviation of the local (λ_{PL}) Planck feedback parameter from its global mean: $\lambda_{PL}' = \lambda_{PL} - \overline{\lambda}_{PL}$. As noted by Dai and Jenkins (2023), this estimated warming amount often does not represent a real warming contribution as the TOA flux change (ΔR_i) may not be used to directly raise surface air temperature or the temperature response may be delayed. We average the terms in Eq. (15) over the Arctic (67°–90° N) and the tropics (23.5° S–23.5° N) to estimate the potential warming contribution of each process to surface warming and AA as done previously (Pithan and Mauritsen 2014; Goosse et al. 2018; Stuecker et al. 2018; Hahn et al. 2021). We define the tropical region as 23.5° S–23.5° N as these are the latitude bands between the Tropic of Capricorn and Tropic of Cancer; however, averaging over other latitude ranges for the tropics (e.g., 30° S-30° N) does not impact the results.

3 Results

3.1 Surface warming response to changes in global SST or Arctic SIC

We first examine the annual-mean surface air temperature response to historical and future global SST (Fig. 2a, b) or Arctic SIC (Fig. 2c, d) changes shown in Fig. 1. The globe experiences relatively uniform warming in pdSST-pdSIC relative to piSST-pdSIC (Fig. 2a, referred to as historical warming) and in futSST-pdSIC relative to pdSST-pdSIC (Fig. 2b, referred to as future warming), with slightly greater magnitude in the future SST case than the historical case. Thus, the SST perturbation runs show background global warming without noticeable AA. In contrast, reduced Arctic sea-ice leads to large warming over Arctic oceanic areas with little temperature change south of ~ 60°N and over northern high latitude land surfaces in both the historical and future perturbed SIC runs (Fig. 2c, d). Note that the local Arctic warming is larger for the future case than the historical case as the future sea-ice loss is larger (Fig. 1c, d) and that the largest historical warming (Fig. 2c) occurs over the Barents-Kara Seas region where there is large sea-ice loss (Fig. 1b).

The seasonal cycle of the surface air temperature changes averaged over the Arctic (Fig. 3a) and globe (Fig. 3b) shows different responses to global SST or Arctic SIC perturbations. Global SST perturbations produce small Arctic warming during historical (~ 0.5–1.0 K) and future (~ 1.0–2.0 K) periods for October–March and summer warming in the future global SST perturbation simulation is larger than the future Arctic SIC experiment (Fig. 3a). The global-mean surface temperature warms by ~ 0.8 K for the historical and ~ 1.2 K for the future SST cases, with little seasonal variation (Fig. 3b). Thus, there is small AA during October–March while the summer Arctic warming is weaker than the global-mean warming in the SST perturbation experiments (Fig. 3c). In contrast, Arctic sea-ice loss produces large Arctic warming from October-January for the historical and future cases, with weak warming in summer (Fig. 3a). Note that the peak warming shifts from October in the historical case to November in the future case. The global-mean warming response to the SIC changes is weak throughout most of the year except during late autumn and early winter (Fig. 3b), which is due to the large warming in the Arctic (Fig. 2c, d). As a result, AA is strong from October-January for the two perturbed SIC cases, especially for the future SIC case (up to 7 K), while the AA is weak during the summer months (Fig. 3c).

3.2 Surface energy budget response to Global SST or local Arctic SIC changes

Increased upward surface energy fluxes over sea-ice retreat areas have been shown to drive large Arctic warming and AA in winter (Deser et al. 2010; Boeke and Taylor 2018; Taylor et al. 2018; Dai et al. 2019). In response to SST warming with fixed SIC, we find little change in the net surface energy flux, net surface SW, SH, and LH fluxes over the Arctic Ocean throughout the year (Fig. 4). The upward net surface LW flux decreases by ~ 1 W m^{-2} for both the historical and future SST warming cases with fixed SIC (Fig. 4c). This represents a small increase in the downward LW radiation, likely due to increased water vapor and enhanced atmospheric energy convergence into the Arctic, rather than changes to surface conditions, as shown below. The suppressed Arctic surface warming and weak oceanic energy flux response to SST warming without SIC changes is consistent with Dai et al. (2019), who found similar results in model simulations with increasing CO_2 concentrations and fixed Arctic sea-ice in flux calculations.

Arctic sea-ice loss greatly influences the magnitude and seasonal cycle of the Arctic oceanic heat flux. From May–August, oceanic *absorption* of energy increases by ~ 6–12 W m^{-2} in response to historical and future SIC loss (Fig. 4a) while during October–March oceanic *release* of energy increases by ~ 12–18 W m^{-2} (Fig. 4a). Most of the increased oceanic energy absorption from May–August is due to increased absorption of SW radiation (Fig. 4b), with negligible changes in net surface LW, SH, and LH fluxes (Fig. 4c-e) during summer. In contrast, net surface LW, SH, and LH fluxes are the main contributors to the enhanced cold-season oceanic energy release in response to Arctic sea-ice loss (Fig. 4d, e). Further, the ocean surface emits more LW radiation to the atmosphere from October–March for historical and future Arctic sea-ice loss runs (Fig. 4c). The

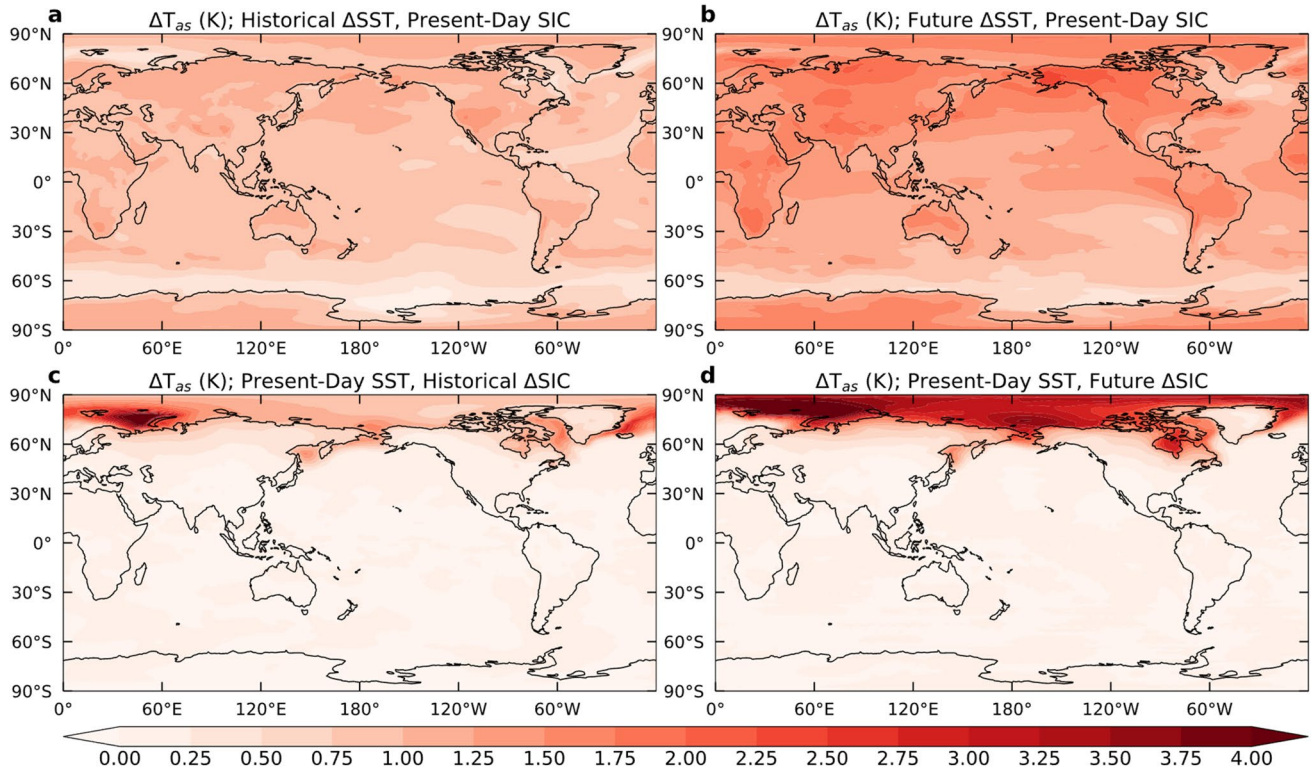

Fig. 2 Multi-model ensemble mean changes in annual-mean surface air temperature (ΔT_{as}) in response to (**a, c** historical and **b, d** future **a, b** SST and **c, d** SIC changes shown in Fig. 1

large increases in upward surface energy fluxes in response to sea-ice loss play an important role in enhancing warming of the surface air and AA during winter (Fig. 3a).

3.3 Feedback seasonal cycles and warming contributions

The contrasting surface warming responses to global SST changes or local sea-ice loss greatly influence Arctic climate feedbacks and atmospheric energy convergence changes. Figure 5 shows the seasonal cycle of TOA radiative contributions of the climate feedbacks and atmospheric energy convergence. Their corresponding climate feedback parameters (i.e., the TOA radiative flux changes normalized by the annual-mean Arctic average surface warming) show similar seasonal cycles (not shown) even though warming is smaller in the SST warming experiment than the SIC loss simulation. Under global SST warming with fixed SIC, Arctic atmospheric energy convergence (Fig. 5f) and water vapor feedback (Fig. 5b) become important contributors to the Arctic TOA flux change. Specifically, atmospheric energy convergence into the Arctic responds similarly to historical and future SST warming, with increases of ~ 4–7 W m^{-2} during October–March and ~ 2–4 W m^{-2} from April-September (Fig. 5f). This suggests that without changes in sea ice, increased atmospheric energy transport becomes an important contributor to small cold season Arctic warming and AA (Fig. 3). Further, the magnitude and seasonal cycle of the water vapor feedback is similar between the historical and future SST cases, with maximum water vapor feedback from May–August and minimum water vapor feedback during October–March (Fig. 5b). This is expected as the warm-season Arctic would see larger water vapor increases due to its warmer mean air temperatures. Arctic surface albedo (Fig. 5a), lapse rate (Fig. 5c), and Planck (Fig. 5d) feedbacks weakly respond to SST increases without sea-ice loss. Lastly, we note that the net cloud feedback produces slight cooling in response to SST increases for June–August (Fig. 5e).

In response to sea-ice loss, Arctic surface albedo feedback increases by ~ 7–8 W m^{-2} and ~ 12–18 W m^{-2} for historical and future cases during the sunlit months (i.e., April-September) due to increased exposure of dark water surfaces (Fig. 5a). The ocean, rather than the atmosphere, absorbs much of the extra SW radiation (Fig. 4a), resulting in weak summer surface warming (Fig. 3a). Cloud feedback is negative in response to sea-ice loss during April-August,

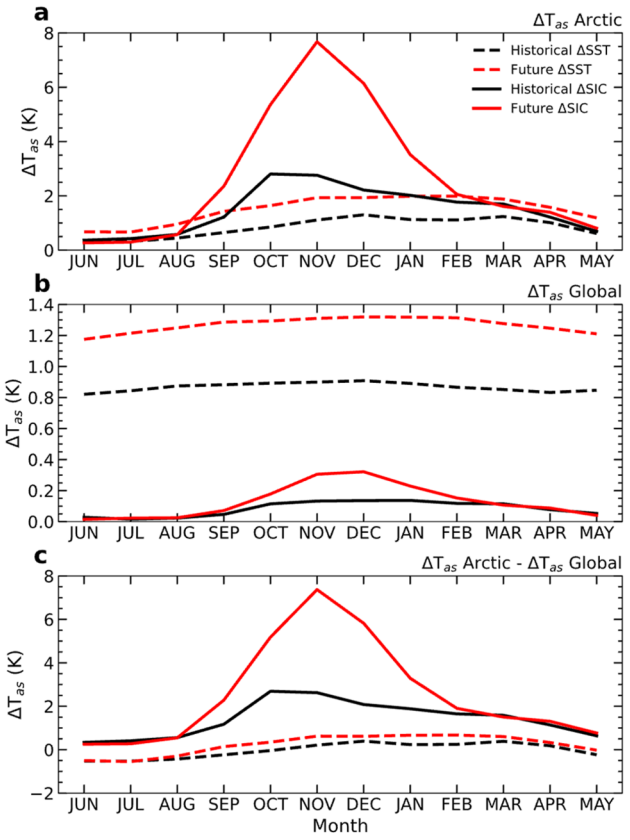

Fig. 3 Multi-model ensemble mean seasonal cycle of surface air temperature changes (ΔT_{as}; in K) in response to historical (black lines) and future (red lines) SST (dashed lines) and SIC (solid lines) perturbations shown in Fig. 1 averaged over the **a** Arctic (67°–90° N) and **b** globe, and **c** Arctic minus global-mean difference (i.e., Arctic amplification). Land surfaces are excluded in (**a**)

and the cooling is larger in the future SIC case (– 1.5 to – 4.5 W m^{-2}) than the preindustrial SIC run (– 1.0 to –1.5 W m^{-2}). Lapse rate (Fig. 5c) and Planck (Fig. 5d) feedbacks weakly respond to historical or future Arctic SIC changes in summer due to small surface warming (Fig. 3a) during the sunlit season. We also find negligible water vapor feedback in response to Arctic sea-ice loss throughout the year, which differs from the noticeable water vapor feedback in response to SST warming (Fig. 5b).

The large cold-season surface warming in response to historical and future Arctic sea-ice loss enhances Arctic lapse rate (Fig. 5c) and Planck (Fig. 5d) feedbacks. When Arctic surface warming (Fig. 3a) and AA (Fig. 3c) peak from October-December, the lapse rate feedback increases the incoming TOA radiative flux by ~ 4–6 W m^{-2} (~ 8–11 W m^{-2}) and the Planck feedback opposes warming by -6 ~ -8 W m^{-2} (-16 ~ -20 W m^{-2}) due to historical (future) sea-ice loss. Note that the month of maximum (minimum) lapse rate (Planck) feedback in the historical and future SIC cases (Fig. 5c) corresponds to the month of peak Arctic surface warming (Fig. 3a), which in turn is related to peak oceanic heating (Fig. 4a) induced by sea-ice loss (Fig. 4f) in these simulations. The cloud feedback in response to future Arctic sea-ice loss also enhances the net incoming TOA radiative flux from October-January by ~ 2.5–3.0 W m^{-2}, but the cloud feedback is weak (< 1.0 W m^{-2}) during winter in response to historical sea-ice loss (Fig. 5e). In contrast to the SST change simulations, Arctic atmospheric energy convergence weakens by ~ 4 W m^{-2} and ~ 7 W m^{-2} in response to historical and future sea-ice loss from November–December, respectively (Fig. 5f). Enhanced Arctic warming in response to sea-ice loss in the non-summer months (Fig. 3a) weakens the temperature gradient between the midlatitudes and polar regions, thus reducing atmospheric energy convergence into the Arctic region.

Warmer SSTs enhance poleward atmospheric energy transport at all latitudes for each model for the historical (Fig. 6a) and future (Fig. 6b) SST warming cases, with slightly larger increases in the northern hemisphere than southern hemisphere from October–March. All models, except CESM2, show enhanced cold season northward energy transport with peak increases of around ~ 45°–50° N for the SST warming cases. In CESM2, atmospheric energy transport shows maximum increases around 30° N for October–March. Thus, without large Arctic warming related to sea-ice loss, the atmosphere displaces energy surpluses poleward. For the SIC perturbation experiments, there is a net decrease in poleward atmospheric energy transport around 30°–90° N with a maximum decrease around 60° N but little change south of 30° N for both historical (Fig. 6c) and future (Fig. 6d) sea-ice loss, consistent with previous studies (Deser et al. 2015; Audette et al. 2021). Again, CESM2 is an outlier compared to the rest of the models for the future ΔSIC run as northward atmospheric energy transport increases from 30° to 60° N (Fig. 6d) for this model. Therefore, SST-induced background warming enhances atmospheric poleward energy transport into the polar regions, while large Arctic warming in response to sea-ice loss weakens atmospheric poleward energy transport over the northern mid-high latitudes.

Figure 7 shows the *potential* warming contributions of the climate feedbacks over the Arctic and the tropics for October–March as AA is largest in autumn and winter. We recognize that warm season feedbacks indirectly affect Arctic surface warming in winter by increasing summer oceanic energy storage that is later released to the atmosphere in the cold season (Dai 2021). Atmospheric energy convergence is the largest contributor for October–March (Fig. 7a, b) Arctic warming under historical (Fig. 7a) and future (Fig. 7b) global SST changes, as it redistributes the energy from the lower latitude oceans, where SSTs increase, to the Arctic region. In contrast, oceanic heat release opposes AA in response to global SST warming for October–March

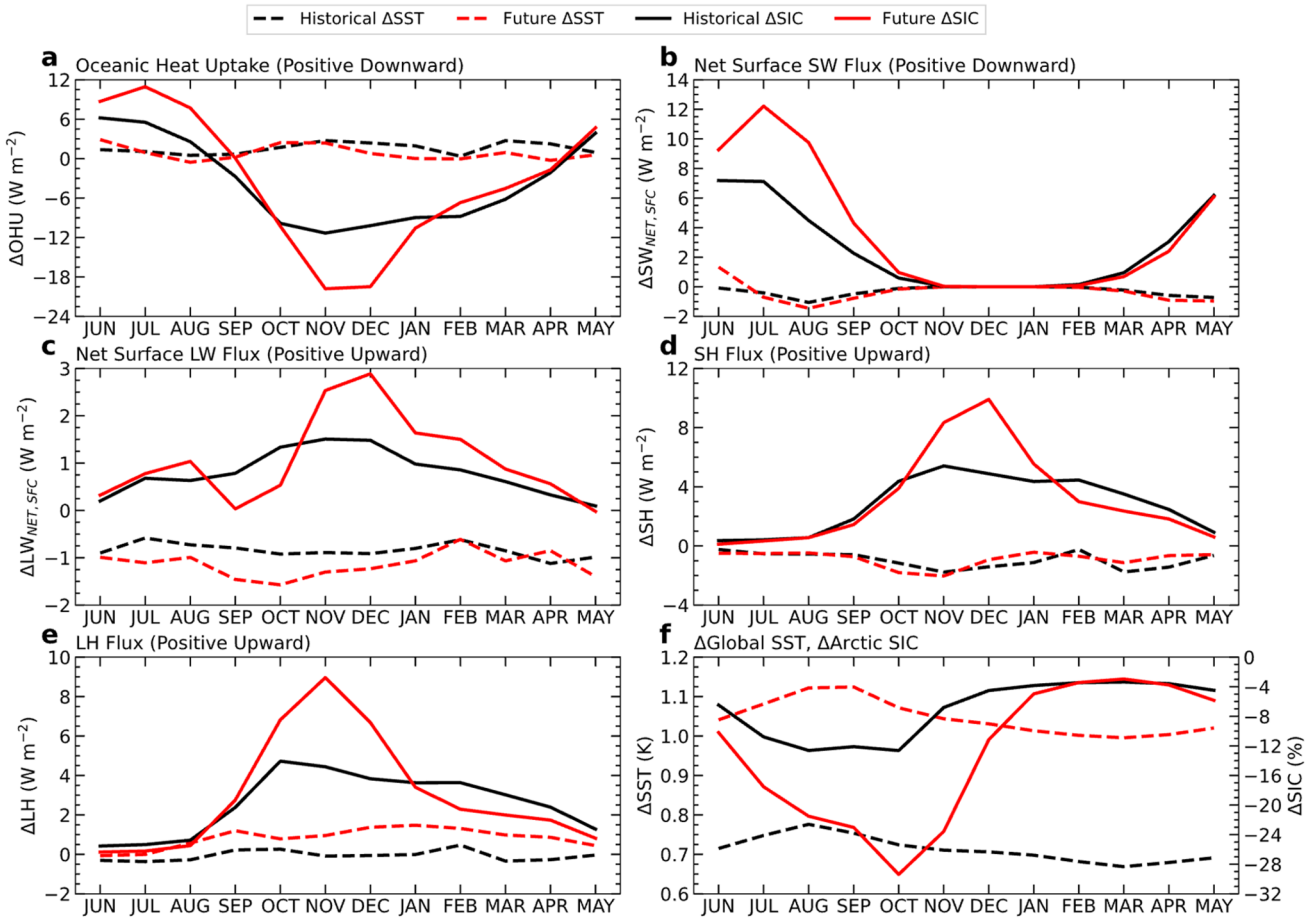

Fig. 4 Arctic (67°–90° N) multi-model ensemble mean seasonal cycle of changes in **a** OHU (positive downward), **b** net surface SW flux (positive downward), **c** net surface LW flux (positive upward), **d** SH flux (positive upward), and **e** LH flux (positive upward) in response to historical (black lines) and future (red lines) SST (dashed lines) and SIC (solid lines) perturbations shown in Fig. 1. All values are in W m^{-2} and land surfaces are excluded from averages. **f** The seasonal cycle of the historical (black lines) and future (red lines) global SST changes (left y-axis; dashed lines) and Arctic SIC loss (right y-axis; solid lines) specified in the SIC and SST perturbation experiments

(Fig. 7a, b) because the warmer SSTs produce a greater ocean-to-atmosphere energy flux outside the Arctic, thus causing more warming in the tropics than in the Arctic. We note that the warming contribution of -ΔOHU in the tropics and cooling effect of -ΔOHU in the Arctic may be related to reduced poleward oceanic heat transport that is implicitly included in the historical and future SST fields. However, analyses of simulations with a coupled atmosphere–ocean are needed to confirm the role of oceanic heat transport on Arctic and tropical warming. Water vapor feedback makes a small contribution to Arctic warming due to low October–March mean temperatures but contributes to ~ 1 K of warming in the tropics in response to global SST warming (Fig. 7b), opposing AA. Without sea-ice loss, lapse rate feedback contributes little to Arctic warming but produces weak tropical cooling in response to historical (Fig. 7a) and future (Fig. 7b) SST increases for the cold season. The local Planck feedback (relative to the global-mean Planck feedback) slightly contributes to AA in the SST warming runs because the cooling effects from Planck feedback are slightly less in the Arctic region than over the rest of the world (Fig. 7). Surface albedo feedback contributes to negligible Arctic warming or AA from October–March in response to global SST increases and fixed Arctic SIC during for historical (Fig. 7a) and future (Fig. 7b) cases.

In response to Arctic sea-ice loss with fixed global SSTs, oceanic heat release is the largest contributor to AA from October–March in historical (Fig. 7c) and future (Fig. 7d) SIC cases, followed by the positive lapse rate feedback. This supports previous studies that showed that sea-ice loss and oceanic energy release during Arctic winter are necessary to trigger large surface warming and thus strong positive lapse rate feedback in the Arctic (Feldl et al. 2020; Jenkins and Dai 2021; Dai and Jenkins 2023). The local Planck feedback (relative to the global-mean Planck feedback) also contributes to Arctic warming and AA in response to historical

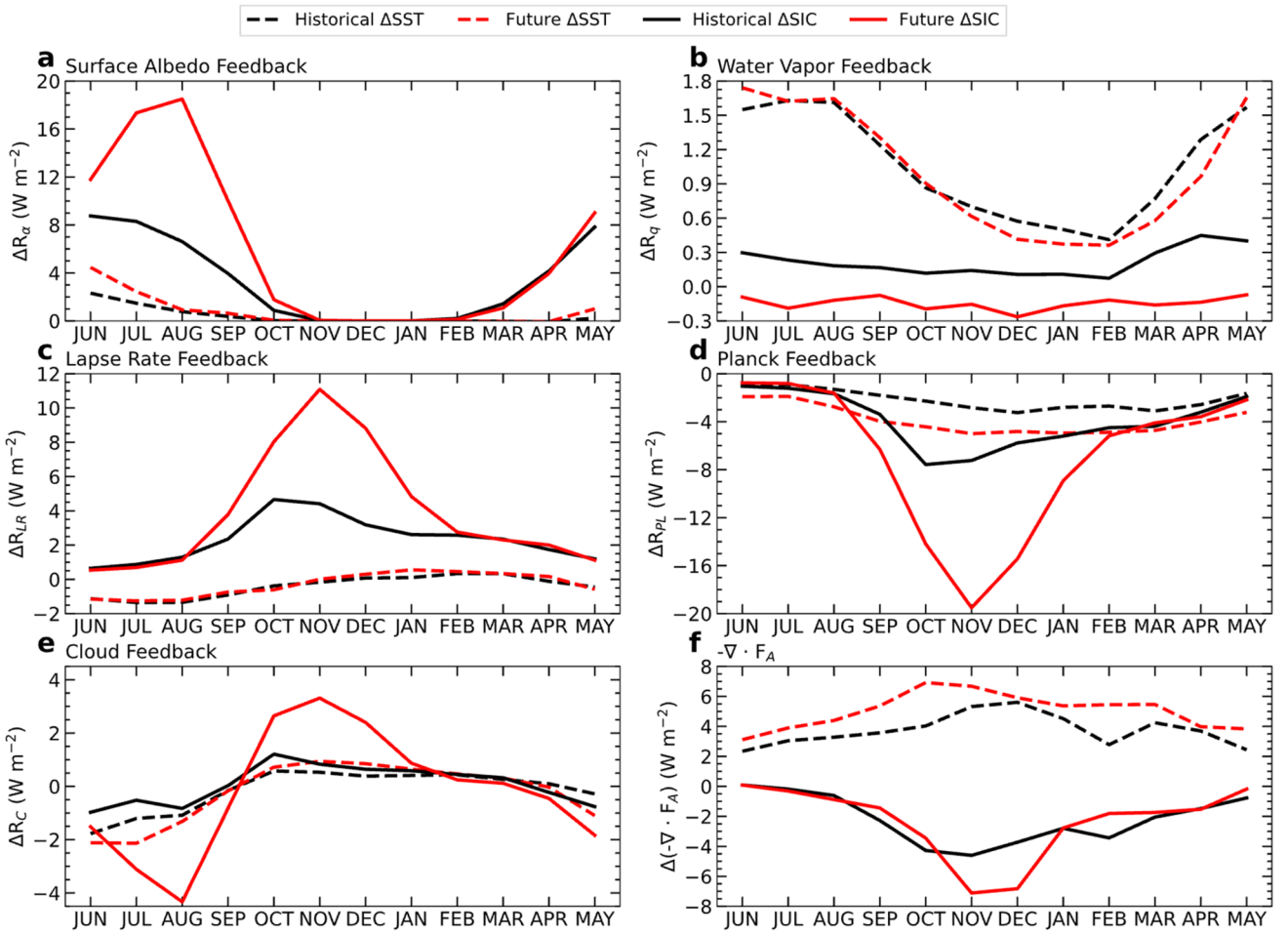

Fig. 5 Arctic (67°–90° N) multi-model ensemble mean seasonal cycle of the **a** surface albedo, **b** water vapor, (**c**) lapse rate, **d** Planck, and **e** cloud feedbacks, and **f** changes in atmospheric energy convergence into the Arctic in response to historical (black lines) and future (red lines) SST (dashed lines) and SIC (solid lines) changes shown in Fig. 1. All values are in W m^{-2} and land surfaces are excluded in averages except for the case shown in (**f**)

(Fig. 7c) and future (Fig. 7d) Arctic SIC changes by cooling the Arctic region less than the tropics. Additionally, positive cloud feedback makes a slight contribution to cold-season Arctic warming and AA in response to future Arctic SIC loss (Fig. 7d), but the contribution is negligible in the historical SIC loss run (Fig. 7c). Water vapor feedback is suppressed over the Arctic and globe in the historical (Fig. 7c) and future (Fig. 7d) SIC runs, suggesting that local sea-ice loss and water vapor feedback are decoupled, as found previously (Jenkins and Dai 2021). In contrast to the perturbed SST runs, the atmosphere displaces energy away from the Arctic in response to cold season sea-ice loss (Fig. 7c, d), thus opposing AA.

Note that warming contributions from changes in oceanic heat release (-ΔOHU) and changes in Arctic atmospheric energy convergence in response to historical (Fig. 7a) and future (Fig. 7b) SST warming in CESM2 differ from the other models during October–March. Specifically, CESM2 oceanic heat release slightly contributes to Arctic warming whereas in the other models, oceanic heat release contributes to Arctic cooling. Due to the warming effect of the – ΔOHU term in response to SST changes in CESM2, Arctic atmospheric energy convergence increases less than the other models (Fig. 7a, b). Further, CESM2 -ΔOHU makes a weaker positive contribution to AA during October–March in response to historical (Fig. 7c) and future (Fig. 7d) Arctic SIC perturbations. Atmospheric energy convergence thus opposes AA less in CESM2 than the other models as -ΔOHU produces less Arctic warming in CESM2 than the other models. These results suggest that changes in Arctic oceanic heat release and changes in atmospheric energy transport are coupled, as noted in previous studies (Hwang et al. 2011; Jenkins and Dai 2021; Dai and Jenkins 2023; Hahn et al. 2023). We note that more work is needed to understand these differences between CESM2 and the other models.

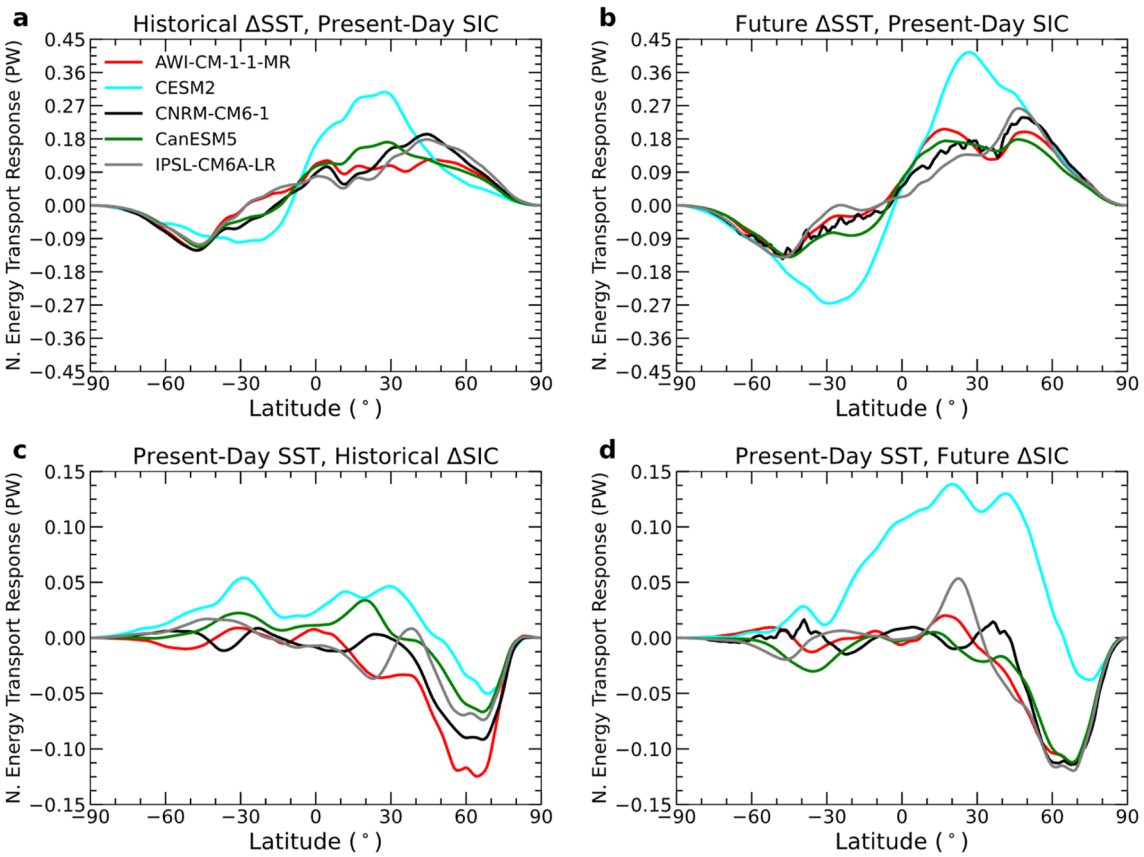

Fig. 6 Changes in October–March mean northward energy transport in response to **a**, **c** historical and **b**, **d** future **a**, **b** SST and **c**, **d** SIC changes shown in Fig. 1

3.4 Physical processes underlying climate feedbacks

Water vapor feedback is complicated in high latitudes due to local temperature inversions and low amounts of water vapor (Curry et al. 1995; Sejas et al. 2018). Global maps reveal that SST warming (Fig. 8a, b) has a larger effect than local sea-ice loss (Fig. 8c, d) on water vapor feedback in both the Arctic and the rest of the globe. Specifically, water vapor feedback is largest near the equator at ~ 2–5 W m^{-2} in response to historical (Fig. 8a) and future (Fig. 8b) SST warming and decreases poleward to ~ 0.5–1.0 W m^{-2} in the Arctic region (Fig. 8a, b). The cold-season water vapor feedback is weak in response to Arctic sea-ice loss (Fig. 8c, d), including over the Arctic where low-level specific humidity increases (Fig. 9c, d). This is due to low or negative values of the October–March LW and net (i.e., LW + SW) water vapor kernel in the Arctic lower troposphere (Fig. 10a, c). Because the water vapor feedback is most sensitive to upper tropospheric water vapor content (Shell et al. 2008; Soden et al. 2008; Pendergrass et al. 2018), the low-level water vapor increases in response to Arctic sea-ice loss do not lead to large TOA flux changes.

Slight positive water vapor feedback occurs over sea-ice loss areas in the historical SIC loss run (~ 0.50–0.75 W m^{-2}; Fig. 8c) but there are negligible water vapor feedback effects in the Arctic under future SIC conditions (Fig. 8d). As the October–March LW and net water vapor kernel is negative near the surface (Fig. 10a, c) due to temperature inversions in the Arctic (Shell et al. 2008; Soden et al. 2008), any increase in moisture in the lower troposphere will result in enhanced radiative emission to space (i.e., a negative water vapor radiative effect). In response to future Arctic SIC (Fig. 9d), there are greater increases in the natural logarithm of specific humidity [Δln(q)] in the lower troposphere than in the historical case (Fig. 9c). Thus, greater future lower tropospheric moistening in the Arctic region produces a more negative water vapor radiative effect at the TOA. We also note that there is a large spread (as shown by the standard deviation) among the PAMIP models and individual ensemble members in upper tropospheric moistening in the perturbed Arctic SIC runs, where there is little change in the mean Δln(q) (Fig. 9c, d). Thus, some ensemble members may have experienced a slight decrease in upper tropospheric Δln(q) in response to Arctic sea-ice loss with fixed global SST,

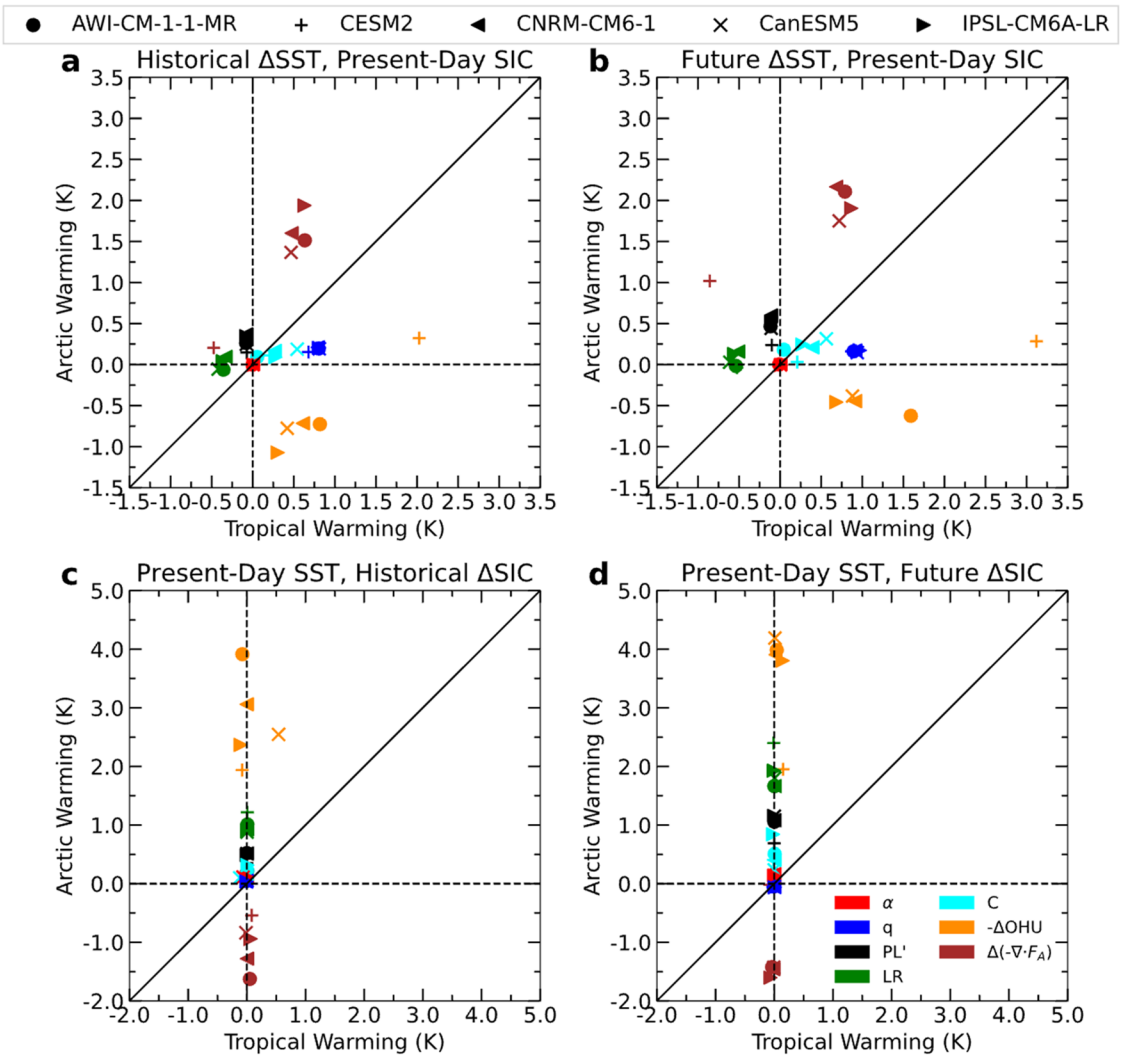

Fig. 7 Inter-model spread in ensemble mean, October–March *potential* warming contributions (in K) of Arctic (67°–90° N) vs. tropical (23.5° S–23.5° N) surface albedo (α), water vapor (q), Planck (PL'), lapse rate (LR), and cloud (C) feedbacks, and changes in oceanic heat release (-ΔOHU; positive upwards), and atmospheric energy convergence ($\Delta(-\nabla \bullet \boldsymbol{F}_A)$) in response to **a**, **c** historical and **b**, **d** future **a**, **b** SST and **c**, **d** SIC perturbations shown in Fig. 1

enhancing outgoing LW radiation at the TOA. In contrast, the historical (Fig. 10a) and future (Fig. 10b) perturbed SST runs experienced slightly greater Δln(q) in the upper troposphere than the lower troposphere for both warm and cold seasons. Due to positive values of the TOA LW and net Arctic water vapor kernel in the upper troposphere (Fig. 10a, c), top-heavy moistening in response to global SST warming produces a positive water vapor feedback from the TOA perspective. We note that the vertical structure of Δln(q) is greater at each level for April-September in the perturbed SST runs than the changed Arctic SIC simulations. Thus, the vertical moistening profile, in addition to the vertical structure of the water vapor kernel, plays a role for the Arctic summer water vapor feedback in the perturbed SST experiments with fixed Arctic SIC.

Arctic low cloud amount has been suggested to increase during the cold season in response to sea-ice loss due to decreased lower tropospheric stability (Kay and Gettelman 2009; Jenkins et al. 2023), thus affecting Arctic cloud feedback (Vavrus 2004; Morrison et al. 2019; Jenkins and Dai 2022). We find weak October–March cloud feedback in response to perturbed SST with fixed Arctic SIC for historical (Fig. 11a) and future (Fig. 11b) cases, suggesting that remote processes do not greatly impact Arctic cloud feedback in the cold season. On the other hand, Arctic sea-ice loss produces a large positive cloud feedback response in winter, especially in regions with large sea-ice loss and surface warming (Fig. 11c, d). For the run with historical SIC loss, cloud feedback enhances the TOA radiative flux by ~ 2–5 W m^{-2} in the Barents-Kara Seas region and

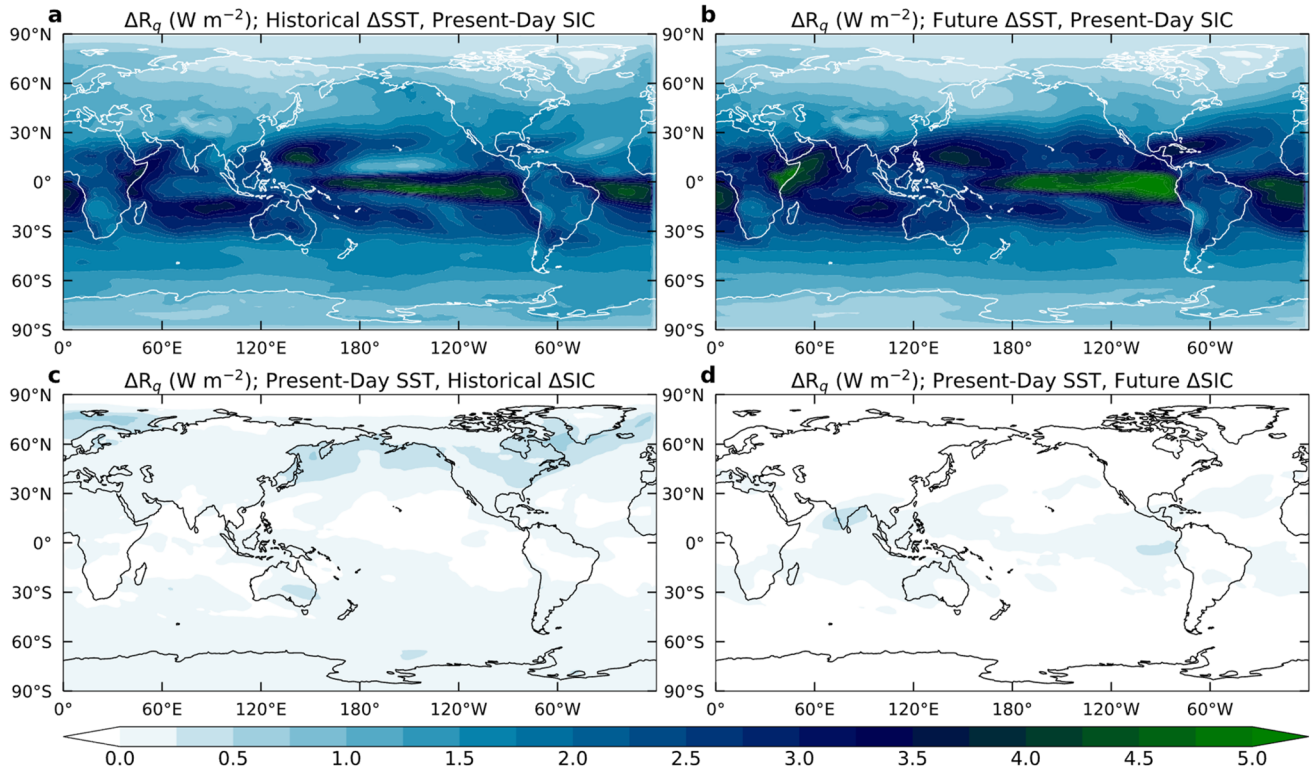

Fig. 8 Multi-model ensemble mean October–March water vapor feedback (in W m^{-2}) in response to **a**, **c** historical and **b**, **d** future **a**, **b** SST and **c**, **d** SIC changes shown in Fig. 1

by ~ 0.5–1.0 W m^{-2} in the Chukchi Sea, where the largest sea-ice loss and surface warming occurs. Under future Arctic sea-ice loss, cold-season cloud feedback is largest in the Barents-Kara Seas (~ 3–5 W m^{-2}) except the warming effects from clouds extend into the Central Arctic Ocean. This is likely related to the greater area with large sea-ice loss (Fig. 1b, d) and surface warming (Fig. 2c-d) in the future case than in the historical case.

The lapse rate feedback experiences large seasonal and spatial variations in the Arctic in response to SST warming or Arctic SIC loss. From October–March, the lapse rate feedback is negative-neutral in response to the global SST warming (Fig. 12a, b) due to relatively uniform vertical warming profiles (Fig. 13a, b). We note that without changes in SIC, there are negligible changes in Arctic oceanic heat uptake or surface warming in the cold season, leading to suppressed lapse rate feedback (Fig. 12a, b). In contrast, cold-season sea-ice loss enhances Arctic lapse rate feedback for historical (Fig. 12c) and future (Fig. 12d) SIC cases when surface and lower tropospheric warming outpaces warming in the mid-upper troposphere (Fig. 13c, d). We note that lapse rate feedback strengthens (~ 6–10 W m^{-2}) in regions with the greatest October–March oceanic heat release and surface warming in response to historical (Fig. 12c) and future (Fig. 12d) sea-ice loss, consistent with previous studies (Dai et al. 2019; Feldl et al. 2020; Boeke et al. 2021; Jenkins and Dai 2021, 2022; Dai and Jenkins 2023). Thus, sea-ice loss is necessary to produce bottom-heavy warming and trigger Arctic positive lapse rate feedback during winter, as shown previously by Dai and Jenkins (2023) using coupled model experiments.

3.5 Response to simultaneous SST and SIC changes

We compare the Arctic vs. tropical October–March potential warming contributions of climate feedbacks, changes in atmospheric energy convergence and oceanic heat release in response to historical global SST warming and historical polar sea-ice loss together (i.e., pdSST-pdSIC minus piSST-piSIC; Fig. 14a; referred to as TOTAL) and the sum of the separate responses to historical SST warming (i.e., pdSST-pdSIC minus piSST-pdSIC) and historical polar sea-ice loss (i.e., pdSST-pdSIC minus pdSST-piArcSIC and pdSST-piAntSIC) (Fig. 14b; referred to as SUM). The warming contributions of the lapse rate, water vapor, cloud, and Planck feedbacks in TOTAL match SUM well, with the lapse rate feedbacks making the largest contribution to AA (Fig. 14). Except for CESM2 in TOTAL, the change

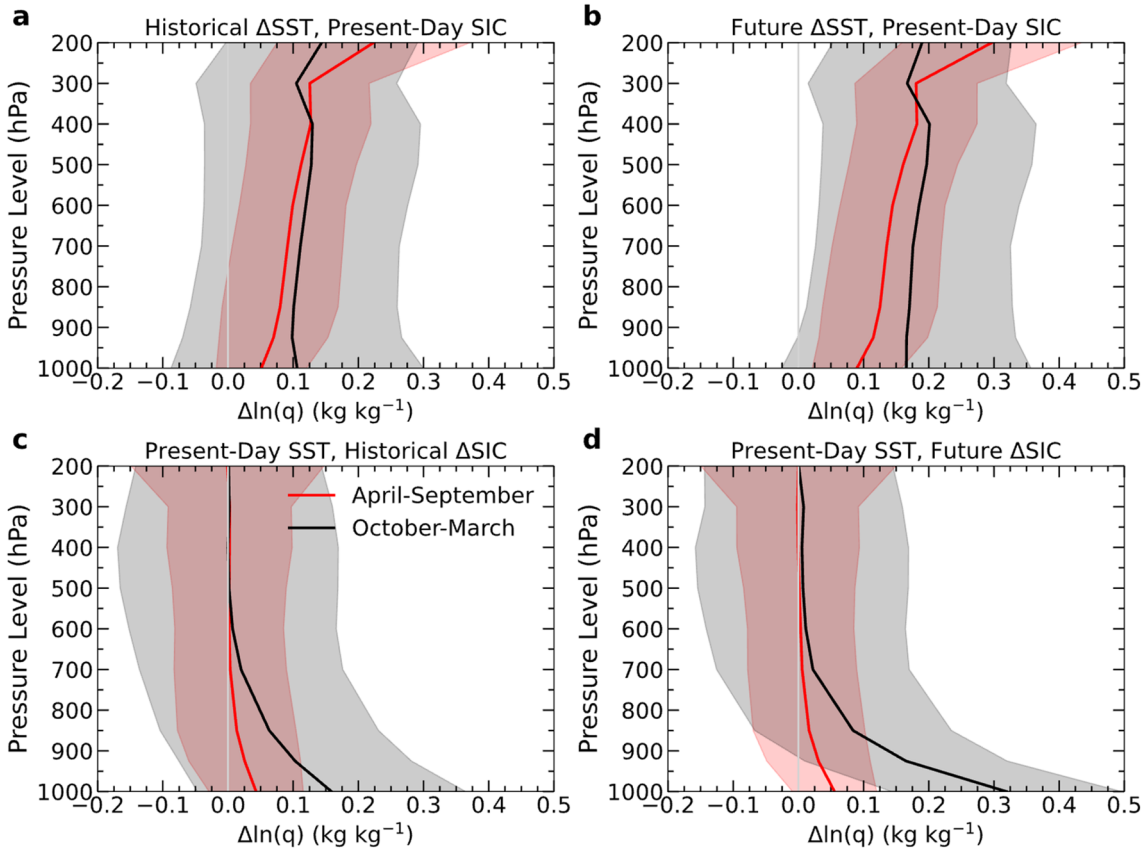

Fig. 9 Multi-model, ensemble mean (solid lines) Arctic (67°–90° N; land surfaces excluded) changes in the natural logarithm of specific humidity (in kg kg^{-1}; solid lines) in response to **a**, **c** historical and **b**, **d** future **a**, **b** global SST and **c**, **d** Arctic SIC changes shown in Fig. 1. The shading shows ± 1 standard deviation from the multi-model ensemble mean profile

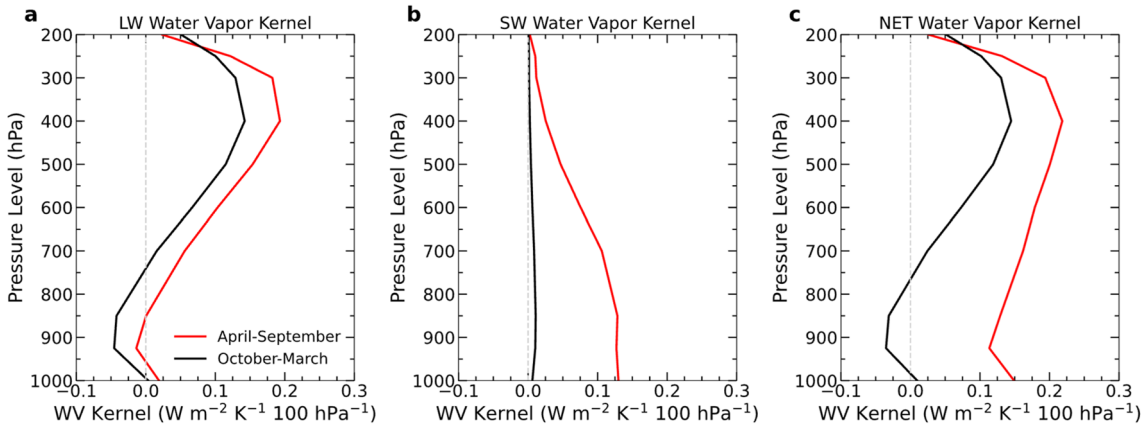

Fig. 10 Profiles of the Pendergrass et al. (2018) TOA **a** LW, **b** SW, and **c** NET (LW + SW) water vapor kernel (in W m^{-2} K^{-1} 100 hPa^{-1}) averaged over the Arctic region (67°–90° N)

in atmospheric energy convergence makes roughly equal warming contributions to Arctic and tropical warming from October–March, suggesting that remote SST warming and Arctic sea-ice loss have opposing effects on the horizontal atmospheric energy flux. The oceanic heat release changes in IPSL-CM6A-LR makes a greater contribution to Arctic than tropical warming, but there are slight discrepancies between CanESM5 and CESM2 oceanic heat release between TOTAL and SUM. In TOTAL, CanESM5 and CESM2 oceanic heat release changes contributes roughly

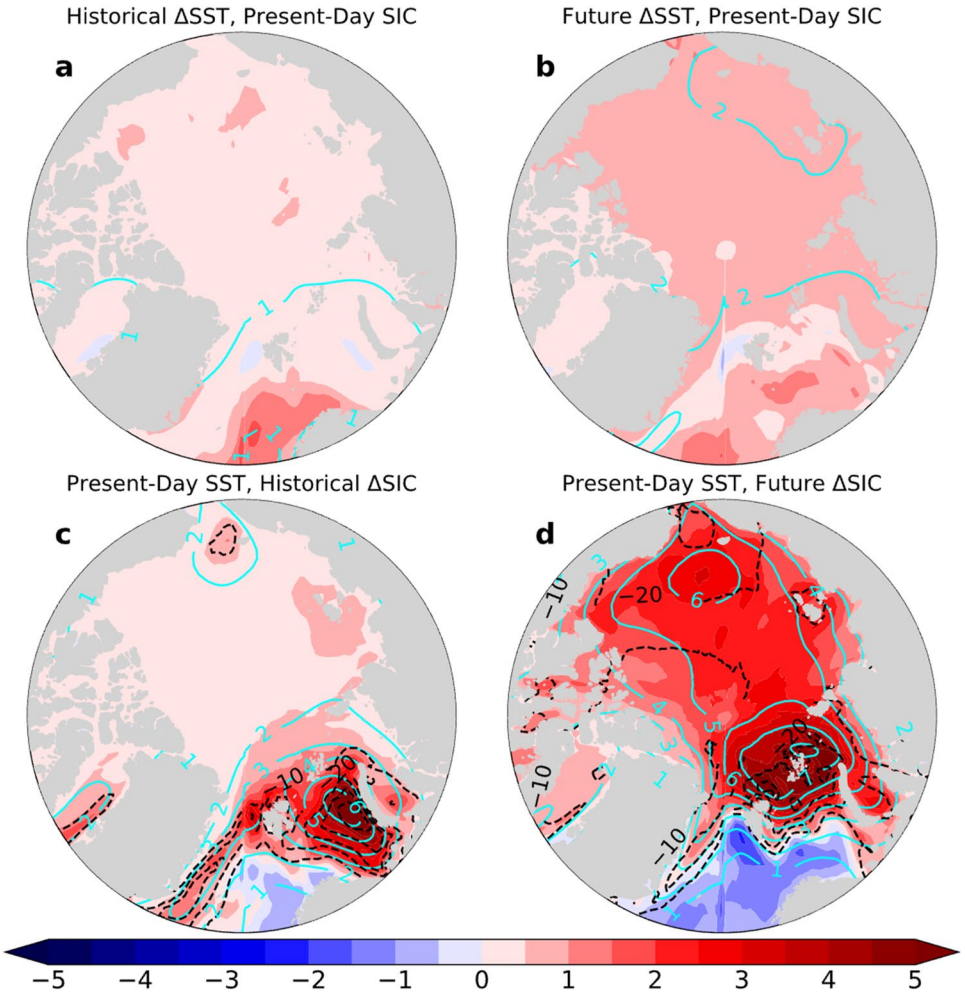

Fig. 11 Multi-model ensemble mean TOA radiative flux change due to the cloud feedback (shading; in W m^{-2}) and change in surface air temperature (cyan contours; in K) averaged over October–March in response to **a, c** historical and **b, d** future **a, b** SST and **c, d** SIC changes. Black contours in (**c**, **d**) show the change in Arctic SIC for October–March

the same amount to Arctic and tropical warming; however, CESM2 (CanESM5) produces slightly greater Arctic (tropical) warming in SUM. The surface albedo feedback is inactive from October–March due to lack of sunlight and is not a major direct contributor to large cold-season AA. The differences between feedbacks calculated with TOTAL and SUM are small except for oceanic heat release and atmospheric energy convergence changes, where there are slight differences in their Arctic vs. tropical warming contributions (Fig. 14c).

The northward atmospheric energy transport response to the SST and SIC perturbations is similar among TOTAL (Fig. 15a) and SUM (Fig. 15b), with little difference between the two cases (Fig. 15c). In the tropical regions (i.e., 30° S-30° N), global SST warming enhances poleward atmospheric energy transport by ~ 0.1–0.15 PW in the southern hemisphere and ~ 0.1–0.35 PW in the northern hemisphere. Around 60°–90° N, there is little net change in atmospheric energy transport in response to simultaneous SST and SIC changes, suggesting that remote warming due to SST changes and local Arctic warming related to sea-ice loss have opposing effects on Arctic atmospheric energy transport (Fig. 6a, c). The similarity of climate feedbacks (Fig. 14) and the atmospheric energy transport (Fig. 15) response between TOTAL and SUM suggest that the effects of SIC or SST changes can be linearly separated. In other words, the individual responses to SST or SIC perturbations approximately sum to the combined influence of changes in SST and SIC.

4 Summary and conclusions

We investigated the impacts of historical and future Arctic sea-ice loss and global SST increases on Arctic climate feedbacks, atmospheric energy convergence into the Arctic, and oceanic heat release using PAMIP atmosphere-only simulations. The SST increase with fixed polar sea ice results in relatively uniform global warming with negligible AA for both historical and future cases. In contrast, historical and future Arctic sea-ice loss leads to large Arctic warming with negligible effects south of ~ 60° N, although this may

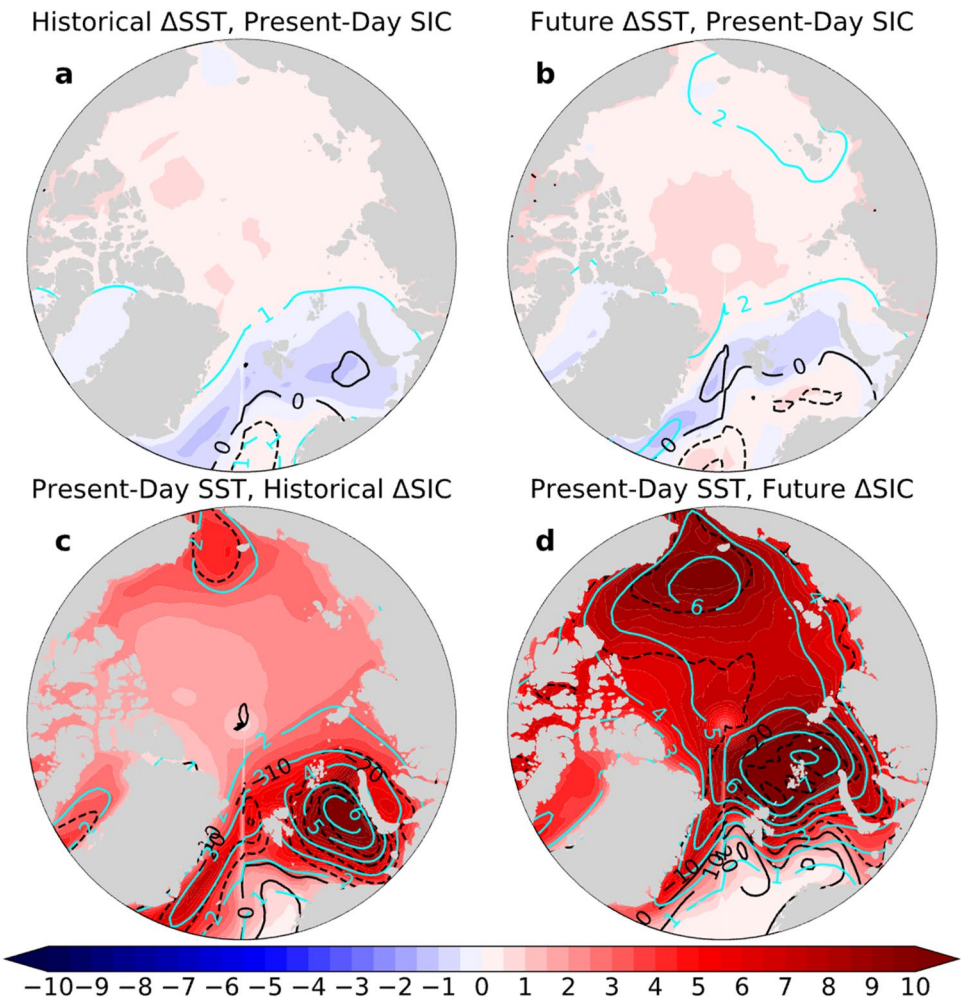

Fig. 12 Multi-model, ensemble mean TOA radiative flux change due to the lapse rate feedback (shading; in W m^{-2}), changes in oceanic heat uptake (black contours; in W m^{-2}; positive downward), and changes in surface air temperature (cyan contours; in K) averaged over October–March in response to **a**, **c** historical and **b**, **d** future **a**, **b** SST and **c**, **d** SIC changes

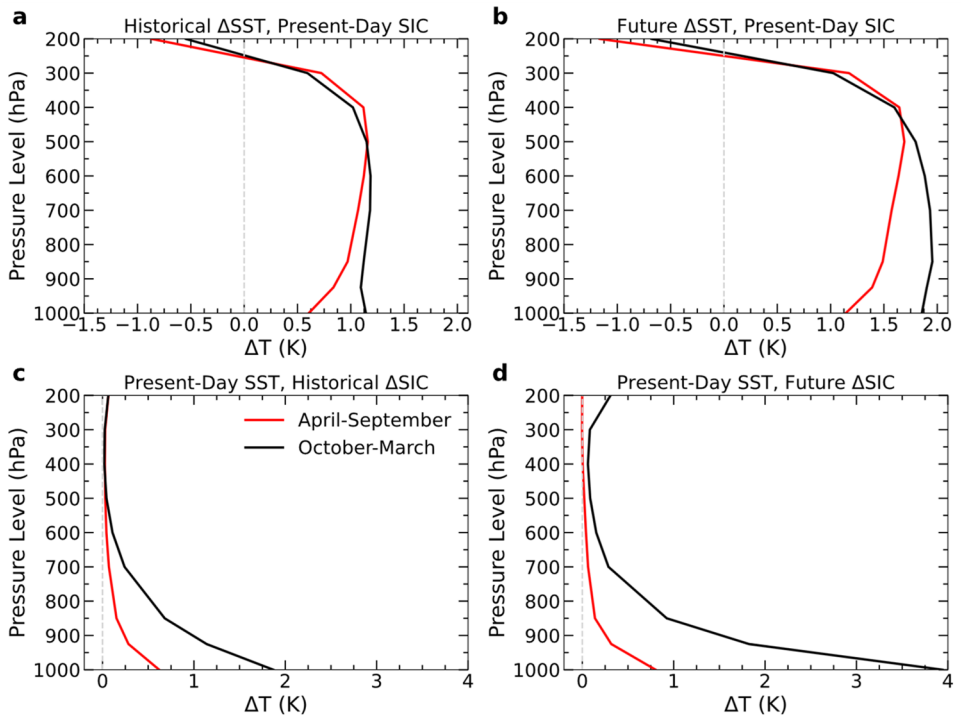

Fig. 13 Multi-model, ensemble mean Arctic (67°–90° N; land surfaces excluded) temperature change profiles (in K) averaged over April-September (red lines) and October–March (black lines) in response to the **a** historical and **b** future global SST warming, and **c** historical and **d** future Arctic sea-ice loss

not be the case in fully coupled simulations (Deser et al. 2015). The PAMIP experiments allowed us to separate the response of Arctic climate feedbacks, atmospheric energy convergence, and oceanic heat release to background global warming without AA (as in the SST perturbation runs) or to large AA with negligible warming outside the Arctic (as in the SIC change runs). We also found striking similarities between the historical simulations with both SST and SIC changes together (i.e., TOTAL), and the sum of the individual responses to the historical SST and polar SIC changes (i.e., SUM) in terms of Arctic climate feedbacks and atmospheric energy transport response.

Under warmer global SSTs without sea-ice loss, Arctic winter oceanic heat release is suppressed leading to weak Arctic cold season warming. Instead, enhanced poleward atmospheric energy convergence rather than increased oceanic heat release becomes the dominant contributor to *small* AA in response to global SST increases with fixed Arctic sea-ice. We also found strong global water vapor feedback in the historical and future SST warming runs, especially in the tropics. Water vapor feedback and moisture intrusions into the Arctic contributes to slight Arctic surface warming by enhancing downwelling LW radiation to the surface (Taylor et al. 2013; Sejas et al. 2014; Song et al. 2014; Yoshimori et al. 2014; Laîné et al. 2016). However, the combined direct effects of enhanced atmospheric energy convergence into the Arctic and positive water vapor feedback produce weak Arctic warming without large sea-ice loss and enhanced oceanic heat release from October–March. We also found that under global SST warming with fixed Arctic SIC, the Arctic experiences vertically uniform or top-heavy warming, producing a neutral or negative lapse rate feedback. Thus, the lapse rate feedback does not make a large contribution to Arctic warming or AA without the bottom-heavy warming effects of enhanced oceanic energy release associated with sea-ice loss. Lastly, Arctic cloud and surface albedo feedbacks responded weakly to warmer global SST with fixed Arctic SIC in the historical and future cases.

In contrast, retreating sea ice produces strong bottom-heavy warming and moistening in autumn and winter due to enhanced oceanic energy release in regions with newly exposed water surfaces, as shown in previous studies (Deser et al. 2010; Screen and Simmonds 2010a, b; Boeke and Taylor 2018; Dai et al. 2019; Dai and Jenkins 2023). Strong lower tropospheric warming enhances Arctic positive lapse rate feedback, which greatly contributes to AA during the cold season (e.g., Jenkins and Dai 2021; Dai and Jenkins 2023). Additionally, bottom-heavy moistening in response to Arctic sea-ice loss has little impact on the TOA radiative flux due to its low sensitivity to lower tropospheric water vapor (Shell et al. 2008; Soden et al. 2008; Pendergrass et al. 2018). Instead, enhanced moistening in the mid-upper troposphere, as in the SST warming runs, increases the Arctic TOA radiative forcing by increasing water vapor's LW absorption in the upper troposphere. Arctic surface albedo feedback activates during the sunlit season in response to sea-ice loss but does not significantly raise surface temperatures in summer. We also find reduced poleward atmospheric energy transport in the northern hemisphere mid-high latitudes due to historical and future Arctic sea-ice loss with fixed global SST, consistent with Hahn et al. (2023).

We recognize that there are limitations associated with atmosphere-only model runs as the ocean is treated as a boundary condition. Ocean–atmosphere coupling and the oceanic component of the poleward energy transport have been shown to play important roles in the atmospheric response to sea-ice loss (Deser et al. 2015; Tomas et al.

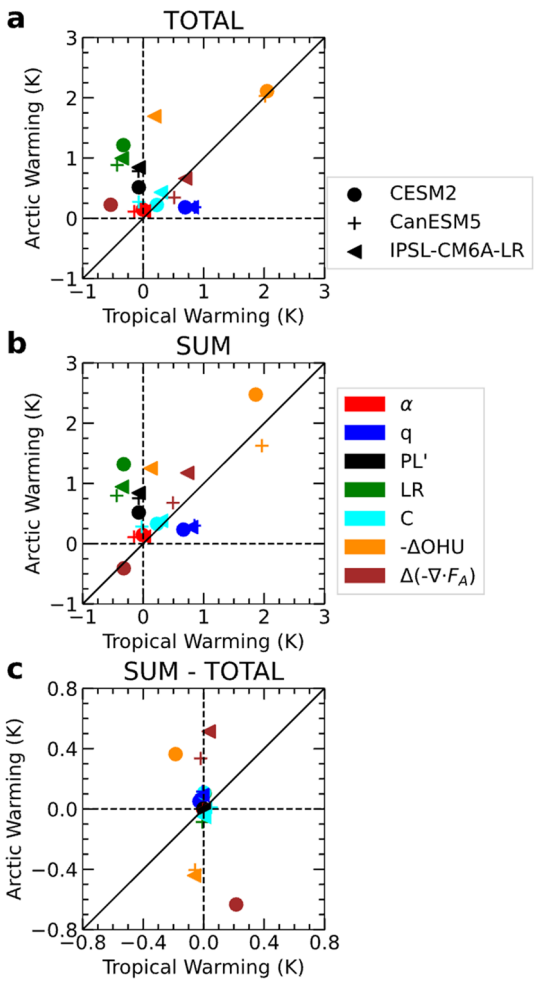

Fig. 14 Inter-model spread in the ensemble mean October–March *potential* warming contributions (in K) for Arctic (67°–90° N) and tropical (23.5° S–23.5° N) surface albedo (α), water vapor (q), Planck (PL'), lapse rate (LR), and cloud (C) feedbacks, and changes in oceanic heat release (-ΔOHU; positive upwards) and atmospheric energy convergence ($\Delta(-\nabla \bullet \boldsymbol{F_A})$) in response to historical changes in global SST and polar SIC for **a** TOTAL (i.e., global SST and polar SIC change together), **b** SUM (i.e., sum of the response to the SST and SIC change separately), and (**c**) difference between (**b**, **a**)

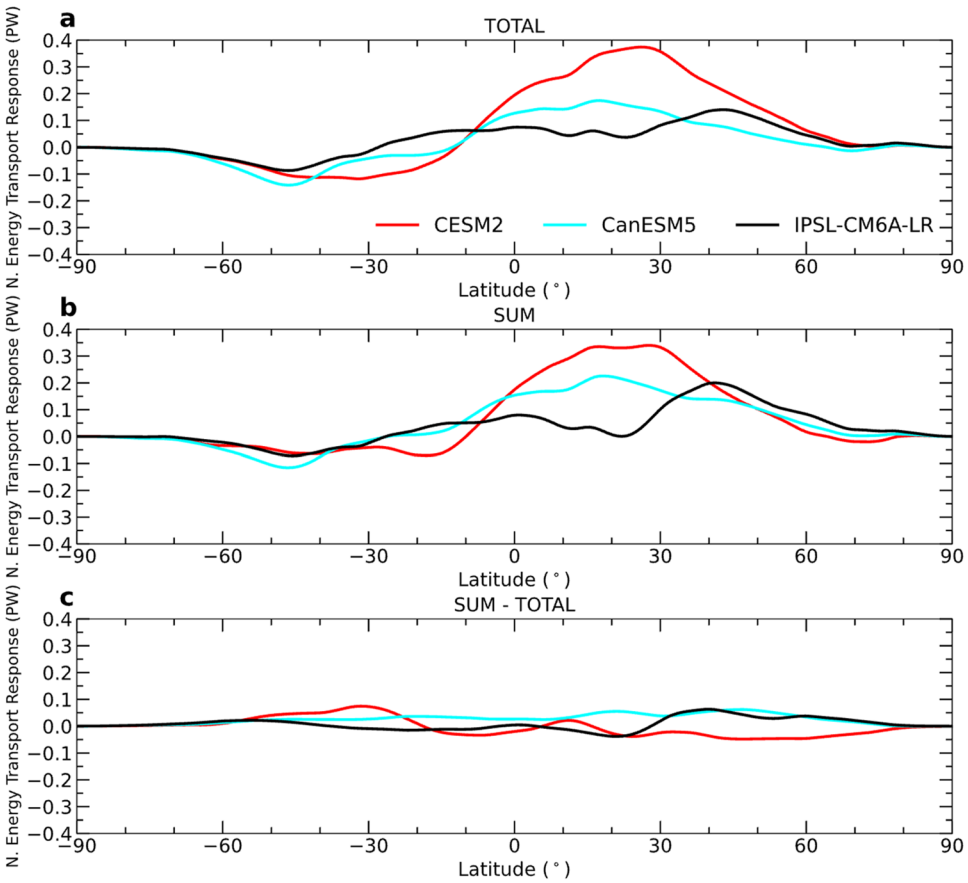

Fig. 15 October–March northward energy transport response (in PW) in response to historical changes in SST and SIC for **a** TOTAL and **b** SUM, and **c** difference between (**b**, **a**)

2016). Thus, future work may compare our feedback calculations to the results from models with a full-depth dynamical ocean to account for ocean feedbacks. Additionally, we emphasize that global SST and Arctic SIC conditions are specified in PAMIP simulations and that many processes influence global SST and Arctic SIC fields in fully-coupled simulations. For example, increased downwelling LW radiation from moisture intrusions into the Arctic or enhanced Arctic atmospheric energy convergence can shape the patterns of future SIC specified in PAMIP simulations (Woods and Caballero 2016; Zhang et al. 2023). Moreover, oceanic heat uptake/release in the simulations with changed SST and fixed SIC may implicitly include changes in oceanic energy convergence as the historical and future SST values were estimated from models with a coupled atmosphere and ocean. Nevertheless, our results help to untangle the influence of background global warming related to global SST changes or large Arctic warming related to sea-ice loss on Arctic climate feedbacks.

Acknowledgements We thank the contributors to the PAMIP project for designing and running the simulations analyzed in this study.

Author contributions M. T. Jenkins performed the analysis for this study, made the figures, and wrote the first draft of the manuscript. A. Dai and C. Deser helped improve the study, the manuscript and the figures.

Funding This work is supported by the National Science Foundation (grants AGS-2015780 and OISE-1743738). The National Center for Atmospheric Research is supported by the National Science Foundation.

Data availability The PAMIP model output used in this study can be downloaded from https://esgf-node.llnl.gov/search/cmip6/.

Declarations

Conflict of interest The authors declare no competing interests.

Ethics approval Not applicable.

Consent for publication The authors agree to publish the paper in *Climate Dynamics*.

References

Alexeev VA, Langen PL, Bates JR (2005) Polar amplification of surface warming on an aquaplanet in "ghost forcing" experiments without sea ice feedbacks. Clim Dyn 24:655–666. https://doi.org/10.1007/s00382-005-0018-3

Audette A, Fajber RA, Kushner PJ, Wu Y, Peings Y, Magnusdottir G et al (2021) Opposite responses of the dry and moist eddy heat transport into the Arctic in the PAMIP experiments. Geophys Res Lett 48:e2020GL089990. https://doi.org/10.1029/2020GL089990

Barton NP, Veron DE (2012) Response of clouds and surface energy fluxes to changes in sea-ice cover over the Laptev Sea (Arctic Ocean). Clim Res 54:69–84. https://doi.org/10.3354/cr01101

Beer E, Eisenman I (2022) Revisiting the role of the water vapor and lapse rate feedbacks in the Arctic amplfication of climate change. J Clim 35:2975–2988. https://doi.org/10.1175/JCLI-D-21-0814.1

Bintanja R, Graversen RG, Hazeleger W (2011) Arctic winter warming amplified by the thermal inversion and consequent low infrared cooling to space. Nat Geosci 4:758–761. https://doi.org/10.1038/ngeo1285

Block K, Mauritsen T (2013) Forcing and feedback in the MPI-ESM-LR coupled model under abruptly quadrupled CO_2. J Adv Model Earth Syst 5:1–16. https://doi.org/10.1002/jame.20041

Boeke RC, Taylor PC (2018) Seasonal energy exchange in sea ice retreat regions contributes to differences in projected Arctic warming. Nat Comm 9:5017. https://doi.org/10.1038/s41467-018-07061-9

Boeke RC, Taylor PC, Sejas SA (2021) On the nature of the Arctic's positive lapse-rate feedback. Geophys Res Lett 48:e2020GL091109. https://doi.org/10.1029/2020GL091109

Burt MA, Randall DA, Branson MD (2016) Dark warming. J Clim 29:705–719. https://doi.org/10.1175/JCLI-D-15-0147.1

Cai M (2005) Dynamical amplification of polar warming. Geophys Res Lett 32:L22710. https://doi.org/10.1029/2005GL024481

Cardinale CJ, Rose BEJ (2023) The increasing efficiency of the poleward energy transport into the Arctic in a warming climate. Geophys Res Lett 50:e2022GL100834. https://doi.org/10.1029/2022GL100834

Chung P-C, Feldl N (2023) Sea ice loss, water vapor increases, and their interactions with atmospheric energy transport in driving seasonal polar amplification. J Clim. https://doi.org/10.1175/JCLI-D-23-0219.1

Colman R, Soden BJ (2021) Water vapor and lapse rate feedbacks in the climate system. Rev Mod Phys 93:045002. https://doi.org/10.1103/RevModPhys.93.045002

Curry JA, Schramm JL, Serreze MC, Ebert EE (1995) Water vapor feedback over the Arctic Ocean. J Geophys Res 100:14223–14229. https://doi.org/10.1029/95JD00824

Dai H (2021) Roles of surface albedo, surface temperature, and carbon dioxide in the seasonal variation of Arctic amplification. Geophys Res Lett 48:e2020GL090301. https://doi.org/10.1029/2020GL090301

Dai A, Jenkins MT (2023) Relationships among Arctic warming, sea-ice loss, stability, lapse rate feedback, and Arctic amplification. Clim Dyn 61:5217–5232. https://doi.org/10.1007/s00382-023-06848-x

Dai A, Luo D, Song M, Liu J (2019) Arctic amplification is caused by sea-ice loss under increasing CO_2. Nat Comm 10:121. https://doi.org/10.1038/s41467-018-07954-9

Davy R, Griewank P (2023) Arctic amplification has already peaked. Environ Res Lett 18:084003. https://doi.org/10.1088/1748-9326/ace273

Deser C, Tomas R, Alexander M, Lawrence D (2010) The seasonal atmospheric response to projected Arctic sea ice loss in the late twenty-first century. J Clim 23:333–351. https://doi.org/10.1175/2009JCLI3053.1

Deser C, Tomas RA, Sun L (2015) The role of ocean-atmosphere coupling in the zonal-mean atmospheric response to Arctic sea ice loss. J Clim 28:2168–2186. https://doi.org/10.1175/JCLI-D-14-00325.1

Dwyer JG, Biasutti M, Sobel AH (2012) Projected changes in the seasonal cycle of surface temperature. J Clim 25:6359–6374. https://doi.org/10.1175/JCLI-D-11-00741.1

Eastman R, Warren SG (2010) Interannual variations of Arctic cloud types in relation to sea ice. J Clim 23:4216–4232. https://doi.org/10.1175/2010JCLI3492.1

England MR, Eisenman I, Lutsko NJ, Wagner TJ (2021) The recent emergence of Arctic amplification. Geophys Res Lett 48:e2021GL094086. https://doi.org/10.1029/2021GL094086

Fasullo JT, Trenberth KE (2008) The annual cycle of the energy budget. Part I: Global mean and land-ocean exchanges. J Clim 21:2297–2312. https://doi.org/10.1175/2007JCLI1935.1

Feldl N, Anderson BT, Bordoni S (2017a) Atmospheric eddies mediate lapse rate feedback and Arctic amplification. J Clim 30:9213–9224. https://doi.org/10.1175/JCLI-D-16-0706.1

Feldl N, Bordoni S, Merlis TM (2017b) Coupled high-latitude climate feedbacks and their impact on atmospheric heat transport. J Clim 30:189–201. https://doi.org/10.1175/JCLI-D-16-0324.1

Feldl N, Po-Chedley S, Singh HKA, Hay S, Kushner PJ (2020) Sea ice and atmospheric circulation shape the high-latitude lapse rate feedback. Npj Clim Atmos Sci 3:41. https://doi.org/10.1038/s41612-020-00146-7

Ghatak D, Miller J (2013) Implications for Arctic amplification of changes in the strength of the water vapor feedback. J Geophys Res Atmos 118:7569–7578. https://doi.org/10.1002/jgrd.50578

Gong T, Feldstein S, Lee S (2017) The role of downward infrared radiation in the recent Arctic winter warming trend. J Climate 30:4937–4949. https://doi.org/10.1175/JCLI-D-16-0180.1

Goosse H, Kay JE, Armour KC, Bodas-Salcedo A, Chepfer H, Docquier D et al (2018) Quantifying climate feedbacks in polar regions. Nat Comm 9:1919. https://doi.org/10.1038/s41467-018-04173-0

Hahn LC, Armour KC, Zelinka MD, Bitz CM, Donohoe A (2021) Contributions to polar amplification in CMIP5 and CMIP6 models. Front Earth Sci 9:710036. https://doi.org/10.3389/feart.2021.710036

Hahn LC, Armour KC, Battisti DS, Eisenman I, Bitz CM (2022) Seasonality in Arctic warming driven by sea ice effective heat capacity. J Clim 35:1629–1642. https://doi.org/10.1175/JCLI-D-21-0626.1

Hahn LC, Armour KC, Battisti DS, Donohoe A, Fajber R (2023) Seasonal changes in atmospheric heat transport to the Arctic under increased CO2. Geophys Res Lett 50:e2023GL105156. https://doi.org/10.1029/2023GL105156

Hall A (2004) The role of surface albedo feedback in climate. J Clim 17:1550–1568. https://doi.org/10.1175/1520-0442(2004)017%3c1550:TROSAF%3e2.0.CO;2

Hay S, Kushner PJ, Blackport R, McCusker KE, Oudar T, Sun L et al (2022) Separating the influences of low-latitude warming and sea-ice loss on northern hemisphere climate change. J Clim 35:2327–2349. https://doi.org/10.1175/JCLI-D-21-0180.1

Henry M, Merlis TM, Lutsko NJ, Rose BEJ (2021) Decomposing the drivers of polar amplification with a single-column model. J Clim 34:2355–2365. https://doi.org/10.1175/JCLI-D-20-0178.1

Hu X, Liu Y, Kong Y, Yang Q (2022) A quantitative analysis of the source of inter-model spread in Arctic surface warming response to increased CO_2 concentration. Geophys Res Lett 49:e2022GL100034. https://doi.org/10.1029/2022GL100034

Hwang Y-T, Frierson DMW (2010) Increasing atmospheric poleward energy transport with global warming. Geophys Res Lett 37:L24807. https://doi.org/10.1029/2010GL045440

Hwang Y-T, Frierson DMW, Kay JE (2011) Coupling between Arctic feedbacks and changes in poleward energy transport. Geophys Res Lett 38:L17704. https://doi.org/10.1029/2011GL048546

Janoski TP, Previdi M, Chiodo G, Smith KL, Polvani LM (2023) Ultrafast Arctic amplification and its governing mechanisms. Environ Res Clim 2:035009. https://doi.org/10.1088/2752-5295/ace211

Jenkins M, Dai A (2021) The impact of sea-ice loss on Arctic climate feedbacks and their role for Arctic amplification. Geophys Res Lett 48:e2021GL094599. https://doi.org/10.1029/2021GL094599

Jenkins MT, Dai A (2022) Arctic climate feedbacks in ERA5 reanalysis: Seasonal and spatial variations and the impact of sea-ice loss. Geophys Res Lett 49:e2022GL099263. https://doi.org/10.1029/2022GL099263

Jenkins MT, Dai A, Deser C (2023) Seasonal variations and spatial patterns of Arctic cloud changes in association with sea-ice loss during 1950–2019 in ERA5. J Climate. https://doi.org/10.1175/JCLI-D-23-0117.1

Kay JE, Gettelman A (2009) Cloud influence on and response to seasonal Arctic sea-ice loss. J Geophys Res 114:D18204. https://doi.org/10.1029/2009JD011773

Kay JE, Holland MM, Bitz CM, Blanchard-Wrigglesworth E, Gettelman A, Conley A et al (2012) The influence of local feedbacks and northward heat transport on the equilibrium Arctic climate response to increased greenhouse gas forcing. J Climate 25:5433–5450

Kay JE, L'Ecuyer T, Chepfer H, Loeb N, Morrison A, Cesana G (2016) Recent advances in Arctic cloud and climate research. Curr Clim Change Rep 2:159–169. https://doi.org/10.1007/s40641-016-0051-9

Kumar A, Perlwitz J, Eischeid J, Quan X, Xu T, Zhang T et al (2010) Contribution of sea ice loss to Arctic amplification. Geophys Res Lett 37:L21701. https://doi.org/10.1029/2010GL045022

Laîné A, Yoshimori M, Abe-Ouchi A (2016) Surface Arctic amplification factor in CMIP5 models: land and oceanic surfaces and seasonality. J Clim 29:3297–3316. https://doi.org/10.1175/JCLI-D-15-0497.1

Liang Y-C, Polvani LM, Mitevski I (2022) Arctic amplification, and its seasonal migration, over a wide range of abrupt CO_2 forcing. Npj Clim Atmos Sci. https://doi.org/10.1038/s41612-022-00228-8

Linke O, Quaas J, Baumer F, Becker S, Chylik J, Dahlke S et al (2023a) Constraints on simulated past Arctic amplification and lapse rate feedback from observations. Atmos Chem Phys 23:9963–9992. https://doi.org/10.5194/acp-23-9963-2023

Linke O, Feldl N, Quaas J (2023b) Current-climate sea ice amount and seasonality as constraints for future Arctic amplification. Environ Res Clim 2:045003. https://doi.org/10.1088/2752-5295/acf4b7

Liu Y, Key JR, Liu Z, Wang X, Vavrus SJ (2012) A cloudier Arctic expected with diminishing sea ice. Geophys Res Lett 39:L05705. https://doi.org/10.1029/2012GL051251

Merlis TM, Henry M (2018) Simple estimates of polar amplification in moist diffusive energy balance models. J Clim 31:5811–5824. https://doi.org/10.1175/JCLI-D-17-0578.1

Middlemas EA, Kay JE, Medeiros BM, Maroon EA (2020) Quantifying the influence of cloud radiative feedbacks on Arctic surface warming using cloud locking in an Earth system model. Geophys Res Lett 47:e2020GL089207. https://doi.org/10.1029/2020GL089207

Monroe EE, Taylor PC, Boisvert LN (2021) Arctic cloud response to a perturbation in sea ice concentration: The north water polynya. J Geophys Res Atmos 126:e2020JD034409. https://doi.org/10.1029/2020JD034409

Morrison AL, Kay JE, Chepfer H, Guzman R, Yettella V (2018) Isolating the liquid cloud response to recent Arctic sea ice variability using spaceborne lidar observations. J Geophys Res Atmos 123:473–490. https://doi.org/10.1002/2017JD027248

Morrison AL, Kay JE, Frey WR, Chepfer H, Guzman R (2019) Cloud response to Arctic sea ice loss and implication for future feedback in the CESM1 climate model. J Geophys Res Atmos 124:1003–1020. https://doi.org/10.1029/2018JD029142

Oort AH, Vonder Haar TH (1976) On the observed annual cycle in the ocean-atmosphere heat balance over the northern hemisphere. J Phys Oceanogr 6:781–800. https://doi.org/10.1175/1520-0485(1976)006%3c0781:OTOACI%3e2.0.CO;2

Palm SP, Strey ST, Spinhirne J, Markus T (2010) Influence of Arctic sea-ice extent and polar cloud fraction and vertical structure and implications for regional climate. J Geophys Res 115:D21209. https://doi.org/10.1029/2010JD013900

Pendergrass AG, Conley A, Vitt FM (2018) Surface and top-of-atmosphere radiative feedback kernels for CESM-CAM5. Earth Sys Sci Data 10:317–324. https://doi.org/10.5194/essd-10-317-2018

Perlwitz J, Hoerling M, Dole R (2015) Arctic tropospheric warming: causes and linkages to lower latitudes. J Climate 28:2154–2167. https://doi.org/10.1175/JCLI-D-14-00095.1

Pithan F, Mauritsen T (2014) Arctic amplification dominated by temperature feedbacks in contemporary climate models. Nat Geosci 7:181–184. https://doi.org/10.1038/NGEO2071

Previdi M, Janoski TP, Chiodo G, Smith KL, Polvani LM (2020) Arctic amplification: A rapid response to radiative forcing. Geophys Res Lett 47:e2020GL089933. https://doi.org/10.1029/2020GL089933

Roe GH, Feldl N, Armour KC, Hwang Y-T, Frierson DMW (2015) The remote impacts of climate feedbacks on regional climate predictability. Nat Geosci 8:135–139. https://doi.org/10.1038/NGEO2346

Schweiger AJ, Lindsay RW, Vavrus S, Francis JA (2008) Relationships between Arctic sea ice and clouds during autumn. J Clim 21:4799–4810. https://doi.org/10.1175/2008JCLI2156.1

Screen JA, Simmonds I (2010a) The central role of diminishing sea ice in recent Arctic temperature amplification. Nature 464:1334–1337. https://doi.org/10.1038/nature09051

Screen JA, Simmonds I (2010b) Increasing fall-winter energy loss from the Arctic Ocean and its role in Arctic temperature amplification. Geophys Res Lett 37:L16707. https://doi.org/10.1029/2010GL044136

Screen JA, Deser C, Simmonds I, Tomas R (2014) Atmospheric impacts of Arctic sea-ice loss, 1979–2009: Separating forced change from atmospheric internal variability. Clim Dyn 43:333–344. https://doi.org/10.1007/s00382-013-1830-9

Sejas SA, Taylor PC (2023) The role of sea ice in establishing the seasonal Arctic warming pattern. Environ Res Clim 2:035008. https://doi.org/10.1088/2752-5295/ace20f

Sejas SA, Cai M, Hu A, Meehl GA, Washington W, Taylor PC (2014) Individual feedback contributions to the seasonality of surface warming. J Clim 27:5653–5669. https://doi.org/10.1175/JCLI-D-13-00658.1

Sejas SA, Taylor PC, Cai M (2018) Unmasking the negative greenhouse effect over the Antarctic Plateau. Npj Clim Atmos Sci 1:17. https://doi.org/10.1038/s41612-018-0031-y

Serreze MC, Barry RG (2011) Processes and impacts of Arctic amplification: A research synthesis. Global Planet Change 77:85–96. https://doi.org/10.1016/j.gloplacha.2011.03.004

Shell KM, Kiehl JT, Shields CA (2008) Using the radiative kernel technique to calculate climate feedbacks in NCAR's community atmospheric model. J Clim 21:2269–2282. https://doi.org/10.1175/2007JCLI2044.1

Smith DM, Screen JA, Deser C, Cohen J, Fyfe JC, García-Serrano J et al (2019) The polar amplification model intercomparison project (PAMIP) contribution to CMIP6: Investigating the causes and consequences of polar amplification. Geosci Model Dev 12:1139–1164. https://doi.org/10.5194/gmd-12-1139-2019

Soden BJ, Held IM, Colman R, Shell KM, Kiehl JT, Shields CA (2008) Quantifying climate feedbacks using radiative kernels. J Climate 21:3504–3520. https://doi.org/10.1175/2007JCLI2110.1

Soldatenko S (2021) Effects of global warming on the poleward heat transport by non-stationary large-scale atmospheric eddies, and feedbacks affecting the formation of the Arctic climate. J Mar Sci Eng 9:867. https://doi.org/10.3390/jmse9080867

Song X, Zhang GJ, Cai M (2014) Quantifying contributions of climate feedbacks to tropospheric warming in the NCAR CCSM3.0. Clim Dyn 42:901–917. https://doi.org/10.1007/s00382-013-1805-x

Stuecker MF, Bitz CM, Armour KC, Proistosescu C, Kang SM, Xie S-P et al (2018) Polar amplification dominated by local forcing and feedbacks. Nat Clim Change 8:1076–1081. https://doi.org/10.1038/s41558-018-0339-y

Sun L, Perlwitz J, Hoerling M (2016) What caused the recent "Warm Arctic, Cold Continents" trend pattern in winter temperatures? Geophys Res Lett 43:5345–5352. https://doi.org/10.1002/2016GL069024

Taylor PC, Monroe E (2023) Isolating the surface type influence on Arctic low-clouds. J Geophys Res Atmos 128:e2022JD038098. https://doi.org/10.1029/2022JD038098

Taylor PC, Cai M, Hu A, Meehl J, Washington W, Zhang GJ (2013) A decomposition of feedback contributions to polar warming amplification. J Clim 26:7023–7043. https://doi.org/10.1175/JCLI-D-12-00696.1

Taylor PC, Kato S, Xu K-M, Cai M (2015) Covariance between Arctic sea ice and clouds within atmospheric state regimes at the satellite footprint level. J Geophys Res Atmos 120:12656–12678. https://doi.org/10.1002/2015JD023520

Taylor PC, Hegyi BM, Boeke RC, Boisvert LN (2018) On the increasing importance of air-sea exchanges in a thawing Arctic: a review. Atmosphere 9:41. https://doi.org/10.3390/atmos9020041

Taylor PC, Boeke RC, Boisvert LN, Feldl N, Henry M, Huang Y et al (2022) Process drivers, inter-model spread, and the path forward: a review of amplified Arctic warming. Front Earth Sci 9:758361. https://doi.org/10.3389/feart.2021.758361

Tomas RA, Deser C, Sun L (2016) The role of ocean heat transport in the global climate response to projected Arctic sea ice loss. J Climate 29:6841–6859. https://doi.org/10.1175/JCLI-D-15-0651.1

Trenberth KE (1997) Using atmospheric budgets as a constraint on surface fluxes. J Climate 10:2796–2809. https://doi.org/10.1175/1520-0442(1997)010%3c2796:UABAAC%3e2.0.CO;2

Trenberth KE, Solomon A (1994) The global heat balance: heat transports in the atmosphere and ocean. Clim Dyn 10:107–134. https://doi.org/10.1007/BF00210625

Vavrus S (2004) The impact of cloud feedbacks on Arctic climate under greenhouse forcing. J Climate 17:603–615. https://doi.org/10.1175/1520-0442(2004)017%3c0603:TIOCFO%3e2.0.CO;2

Virgin JG, Smith KL (2019) Is Arctic amplification dominated by regional radiative forcing and feedbacks: Perspectives from the world-avoided scenario. Geophys Res Lett 46:7708–7717. https://doi.org/10.1029/2019GL082320

Walsh JE (2014) Intensified warming of the Arctic: causes and impacts on middle latitudes. Global Planet Change 117:52–63. https://doi.org/10.1016/j.gloplacha.2014.03.003

Wetherald RT, Manabe S (1988) Cloud feedback processes in a general circulation model. J Atmos Sci 45:1397–1415. https://doi.org/10.1175/1520-0469(1988)045%3c1397:CFPIAG%3e2.0.CO;2

Winton M (2006) Amplified Arctic climate change: What does surface albedo feedback have to do with it? Geophys Res Lett 29:4473–4485. https://doi.org/10.1029/2005GL025244

Woods C, Caballero R (2016) The role of moist intrusions in winter Arctic warming and sea ice decline. J Climate 29:4473–4485. https://doi.org/10.1175/JCLI-D-15-0773.1

Yoshimori M, Wantanabe M, Abe-Ouchi A, Shiogama H, Ogura T (2014) Relative contribution of feedback processes to Arctic amplification of temperature change in MIROC GCM. Clim Dyn 42:1613–1630. https://doi.org/10.1007/s00382-013-1875-9

Zhang P, Chen G, Ting M, Leung LR, Guan B, Li L (2023) More frequent atmospheric river slow the seasonal recovery of Arctic sea ice. Nat Clim Change 13:266–273. https://doi.org/10.1038/s41558-023-01599-3

Zhou S-N, Liang Y-C, Mitevski I, Polvani LM (2023) Stronger Arctic amplification produced by decreasing, not increasing, CO_2 concentrations. Environ Res Clim 2:045001. https://doi.org/10.1088/2752-5295/aceea2